Low-dimensional models for turbulent plane Couette flow in a minimal flow unit

By T. R. SMITH[1] †, J. MOEHLIS[2] ‡, AND P. HOLMES[1,2]

[1]Department of Mechanical and Aerospace Engineering, Princeton University, Princeton, NJ 08544-5263

[2]Program in Applied and Computational Mathematics, Princeton University, Princeton, NJ 08544-1000

(Received 8 December 2003)

We model turbulent plane Couette flow in the Minimal Flow Unit – a domain whose spanwise and streamwise extent is just sufficient to maintain turbulence – by expanding the velocity field as a sum of optimal modes calculated via proper orthogonal decomposition from numerical data. Ordinary differential equations are obtained by Galerkin projection of the Navier-Stokes equations onto these modes. We first consider a 6 mode (11-dimensional) model and study the effects of including losses to neglected modes. Ignoring these, the model reproduces turbulent statistics acceptably, but fails to reproduce dynamics; including them, we find a stable periodic orbit that captures the regeneration cycle dynamics and agrees well with direct numerical simulations. This model, however, fails to reproduce stability of the laminar state, or account for bifurcation to turbulent states as Reynolds number increases. To address these failures, we develop a second class of models based on "uncoupled" eigenfunctions that allow independence among streamwise and cross-stream velocity components. A 9 mode (31-dimensional) model produces bifurcation diagrams for steady and periodic states in qualitative agreement with numerical Navier-Stokes solutions, while preserving the regeneration cycle dynamics. Together, the models provide empirical evidence that the "backbone" for Minimal Flow Unit turbulence is a periodic orbit, and support the roll-streak-breakdown-roll reformation picture of shear-driven turbulence.

1. Introduction

In this paper we continue a study of low-dimensional models of plane Couette flow begun in Moehlis *et al.* (2002). That paper and the present one takes up earlier work begun by Aubry *et al.* (1988); Sanghi & Aubry (1993), cf. Berkooz *et al.* (1991); Podvin & Lumley (1998); Podvin (2001), on near-wall turbulence, in which the proper orthogonal or Karhumen-Loève decomposition (POD), first suggested for use in turbulence by Lumley (1971), is used to construct optimal bases in the sense that truncations at a given order maximally capture kinetic energy on average. The Navier-Stokes equations are (Galerkin) projected onto low-dimensional subspaces spanned by dominant subsets of modes, yielding (relatively) tractable sets of ordinary differential equations (ODEs) for

† Present address: Control and Dynamical Systems, California Institute of Technology, Mail Stop 107-81, 1200 E. California Blvd, Pasadena, CA, 91125, USA.

‡ Present address: Department of Mechanical and Environmental Engineering, University of California, Santa Barbara, CA, 93106, USA.

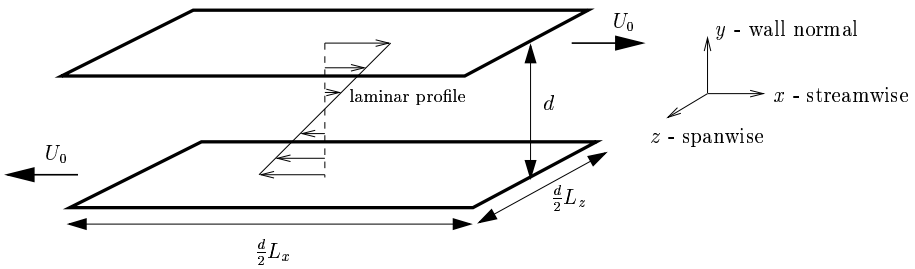

FIGURE 1. Geometry of plane Couette flow (PCF).

the modal amplitudes. The ODEs may then be studied to reveal interactions among coherent structures that, hopefully, form the "backbones" of turbulence. A general account of the strategy, and relevant background information, is given in Holmes *et al.* (1996). In the present paper we address perhaps the simplest turbulent flow, using it to assess the strengths and weaknesses of the low dimensional paradigm.

We consider plane Couette flow in the Minimal Flow Unit (MFU). Here minimality refers to the spanwise and streamwise extents of the spatial domain, which are reduced (in numerical simulations) until turbulence with reasonable statistics is just sustainable. By constraining the flow to a domain that supports only one or two coherent structures, one hopes that the dynamical interactions that sustain turbulence will be sufficiently simplified that better understanding of physical mechanisms will result. Jiminez & Moin (1991) pioneered the idea for turbulent channel flow, and Hamilton *et al.* (1995) subsequently applied it to plane Couette flow. We shall draw heavily on the latter paper, hereafter referred to as HKW, in the comparative studies to follow.

In plane Couette flow (PCF), fluid is sheared between two infinite parallel plates moving at speed U_0, in opposite directions $\pm\mathbf{e}_x$; see Fig. 1. The streamwise, wall-normal, and spanwise directions are respectively x, y, and z. We nondimensionalize lengths in units of $d/2$ where d is the gap between the plates, velocities in units of U_0, time in units of $(d/2)/U_0$, and pressure in units of $U_0^2\rho$ where ρ is the fluid density. Laminar flow is then given by $\mathbf{U}_0 = y\mathbf{e}_x$, $-1 \leqslant y \leqslant 1$ and the Reynolds number is $Re = \frac{U_0 d}{2\nu}$, where ν is the kinematic viscosity. Writing $\mathbf{u} = (u_1, u_2, u_3)$, $\mathbf{x} = (x, y, z)$, the evolution equation for the perturbation $(\mathbf{u}(\mathbf{x}, t), p(\mathbf{x}, t))$ to laminar flow becomes

$$\frac{\partial}{\partial t}\mathbf{u} = -(\mathbf{u}\cdot\nabla)\mathbf{u} - y\frac{\partial}{\partial x}\mathbf{u} - u_2\mathbf{e}_x - \nabla p + \frac{1}{Re}\nabla^2\mathbf{u}. \tag{1.1}$$

The fluid is assumed to be incompressible, i.e.,

$$\nabla\cdot\mathbf{u} = 0, \tag{1.2}$$

with no-slip boundary conditions at the plates, i.e.,

$$\mathbf{u}|_{y=\pm1} = 0, \tag{1.3}$$

and periodicity in the streamwise and spanwise directions, with lengths $L_x = 1.75\pi$ and $L_z = 1.2\pi$, respectively, corresponding to the MFU; see HKW. Our POD bases or empirical eigenfunctions will be derived from a direct numerical simulation (DNS) database computed at $Re = 400$. In Moehlis *et al.* (2002) we took the moderate aspect ratio domain $L_x = 4\pi$, $L_z = 2\pi$, also at $Re = 400$.

Eqns. (1.1-1.3) are equivariant with respect to the following symmetries (Schmiegel

(1999)):

$$\mathcal{P}\cdot[(u_1,u_2,u_3,p)(x,y,z,t)] = (-u_1,-u_2,-u_3,p)(-x,-y,-z,t) \tag{1.4}$$

$$\mathcal{R}\cdot[(u_1,u_2,u_3,p)(x,y,z,t)] = (u_1,u_2,-u_3,p)(x,y,-z,t) \tag{1.5}$$

$$\mathcal{RP}\cdot[(u_1,u_2,u_3,p)(x,y,z,t)] = (-u_1,-u_2,u_3,p)(-x,-y,z,t) \tag{1.6}$$

$$\mathcal{T}_{\Delta x,\Delta z}\cdot[(u_1,u_2,u_3,p)(x,y,z,t)] = (u_1,u_2,u_3,p)(x+\Delta x,y,z+\Delta z,t). \tag{1.7}$$

Thus, if $\mathbf{u}(\mathbf{x},t)$ solves (1.1), the solution obtained by acting on $\mathbf{u}(\mathbf{x},t)$ with any product of the actions given in equations (1.4-1.7) also solves it: e.g., if

$$(u_1(x,y,z,t),u_2(x,y,z,t),u_3(x,y,z,t),p(x,y,z,t))$$

solves (1.1), then so does

$$(u_1(x,-y,z,t),-u_2(x,-y,z,t),u_3(x,-y,z,t),p(x,-y,z,t)).$$

Physically, $\mathcal{P}$ is a point reflection about $(x,y,z)=(0,0,0)$, $\mathcal{R}$ is a reflection about the plane $z=0$, $\mathcal{RP}$ is a rotation by π about the z-axis, and $\mathcal{T}_{\Delta x,\Delta y}$ is a translation by Δx in the streamwise direction and by Δz in the spanwise direction. As described in Moehlis *et al.* (2002), $\mathcal{P}$ and $\mathcal{R}$ generate a four element group isomorphic to the abstract group D_2 (see, e.g., Lomont (1993)), and altogether, with the continuous translations (1.7), the governing equations are equivariant with respect to the direct product $O(2)\times O(2)$. In the empirical-Fourier decomposition developed below, this corresponds to independent rotations and reflections with respect to streamwise and spanwise Fourier wavenumbers. The wall layer model of Aubry *et al.* (1988) shares only *some* of these symmetries, having only $O(2)\times S^1$ symmetry (the upper wall is absent in Aubry *et al.* (1988), thus there is no analog of $\mathcal{P}$ (1.4)). We will use (1.4-1.6) in our application of the POD procedure to create a basis endowed with the appropriate symmetries, and to check subsequently that the projected ODEs preserve them.

We contend that MFU PCF turbulence is a good test case for assessment of low dimensional modeling strategies because the turbulence is relatively mild and involves few structures (thus, if the strategy fails here, it is not likely to succeed in more fully-developed turbulence), and because PCF exhibits numerous interesting properties that a model should reproduce. Specifically, the laminar state $\mathbf{U}_0$ is linearly stable for all Reynolds numbers (Drazin & Reid (1981)), but both experiments and simulations exhibit sustained turbulence for sufficiently high Re ($\gtrsim$ 380-400) and perturbation amplitudes (Dauchot & Daviaud (1995*a*,*b*)). Recent mathematical work (e.g. Baggett & Trefethen (1997); Schmid & Henningson (2000)) has stressed the rôle of non-normal operators in such subcritical transitions (the linearised operator of (1.1) is non-normal: $L^\dagger L \neq LL^\dagger$, where † denotes adjoint), and we shall comment on this below. Moreover, Eqn. (1.1) possesses numerous branches of (unstable) steady states consisting of wavy streamwise vortices and streaks that arise in saddle-node bifurcations above $Re\approx 125$ (Nagata (1990); Clever & Busse (1992); Schmiegel (1999)), and in Schmiegel (1999) it was suggested that turbulence might be a "chaotic repellor" formed from heteroclinic connections among such finite amplitude solutions, as in the wall layer models of Aubry *et al.* (1988). The studies in Moehlis *et al.* (2002) support this conjecture, and we provide further comments below. For additional information, experimental work, and references on PCF, see Bech *et al.* (1995); Komminaho *et al.* (1996).

In their study, HKW identified an almost-periodic regeneration cycle or "self-sustaining process," in which near-wall streaks – elongated regions of spanwise alternating high- and low- speed fluid – are produced by streamwise vortices in a process previously discussed in Kline (1967). The streaks, almost straight initially, develop streamwise waviness as

a result of a linear instability; they then break down and, in doing so, regenerate the streamwise vortices, after which the process begins anew.

We develop two classes of models in this paper, using "coupled" and "uncoupled" expansions. The former employs the vector-valued basis functions (empirical eigenfunctions) delivered directly by the POD, as described in Holmes *et al.* (1996). However, as pointed out by Moffatt (1990), and acknowledged in Holmes (1990); Moehlis *et al.* (2002), this can lead to paradoxical results in which, for example, flows containing only streamwise-invariant modes can extract energy from uniform mean shears such as the laminar Couette solution $\mathbf{U}_0$. In Berkooz *et al.* (1991) it was suggested that decoupling of streamwise and spanwise velocity components might repair this situation, and we use a generalisation of this notion due to Waleffe (1995*b*) to develop uncoupled models. In both cases we use Heisenberg (eddy viscosity) type models to account for energy transfer to the (many) neglected modes.

In §2 we briefly describe the DNS data and the POD procedure and outline properties of the empirical eigenvalues derived from it. §§3-4 forms the heart of the paper; here the coupled and uncoupled models are derived and comparisons with the DNS data made and discussed. In §5 we conclude, and compare our models with other low dimensional models, including those of Waleffe (1995*a*,*b*, 1997) (following HKW) and Eckhardt & Mersmann (1999) for shear flow turbulence. The thesis Smith (2003) contains many additional details and analyses.

2. The database, the POD, and empirical eigenfunctions

2.1. *The numerical method and database*

Following HKW; Kawahara & Kida (2001), we used a modification of the usual velocity-vorticity algorithm for channel flow (Kim *et al.* (1987)). As in HKW, convective terms were advanced by means of a third-order Runge-Kutta routine (Zang & Hussaini (1985); Peyret (2002)), rather than the original second-order Adams-Bashforth method. De-aliased Fourier expansions were employed in the streamwise and spanwise directions and Chebyshev polynomials in the wall-normal direction. A computational grid of $16 \times 33 \times 16$ (streamwise $\times$ wall-normal $\times$ spanwise) was used. To produce the simulation data, we began with random initial conditions at $Re = 625$, allowed the system to converge on the turbulent state, and used the final states as new initial conditions as Re was successively reduced to 400 in decreasing steps. Our code was modified from a channel flow code kindly provided by C.W. Rowley, and validated for PCF by comparison with statistics of HKW; Kawahara & Kida (2001), obtaining agreements within 2.2% for mean velocity and 1.2% for r.m.s. fluctuations (in L^2 norm).

After allowing transients to decay and a statistically stationary (turbulent) state to become established, we ran for 20,000 nondimensional time units, assembling a database of 4000 velocity field snapshots $\{\mathbf{u}(\mathbf{x}, t_j)\}$ by recording every 500th timestep ($\Delta t = 0.01$). To ensure that the ensemble possesses the appropriate discrete symmetries (1.4-1.6), we then quadrupled the number of samples in the database by applying these symmetry operations to create our ensemble. This ensures that the POD modes share the symmetries of the governing equations, even if the "raw" database does not. See Berkooz & Titi (1993); Aubry *et al.* (1993); Moehlis *et al.* (2002).

2.2. *Phenomenology of turbulence in the PCF-MFU*

With a view to comparing velocity fields reconstructed from low-dimensional models with "full" DNS data, we briefly survey the results of HKW and present analogous results from

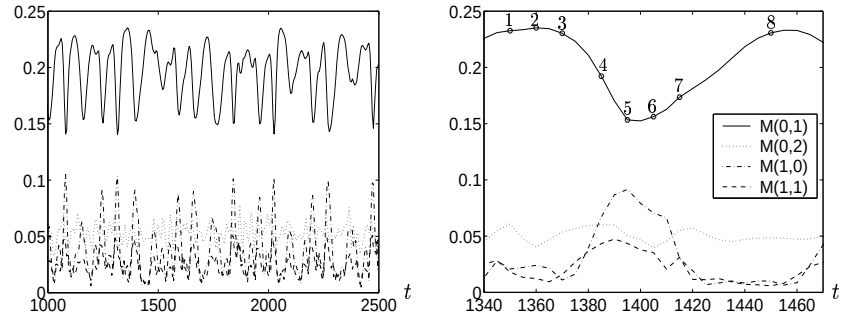

FIGURE 2. The behaviour of the RMS modal velocities, as defined by (2.1), for several wavenumber pairs: over 1500 time units of the DNS (left), and a close-up of one representative cycle (right). Here, and for similar plots throughout this paper, the legend in the right panel also applies to the left panel.

our DNS. In HKW the RMS modal velocities are defined as

$$\mathrm{M}(n_x, n_z) \stackrel{\text{def}}{=} \left(\int_{-1}^{1} \left[\tilde{u}_1^2(n_x, y, n_z) + \tilde{u}_2^2(n_x, y, n_z) + \tilde{u}_3^2(n_x, y, n_z) \right] dy \right)^{1/2}, \tag{2.1}$$

where the tildes represent Fourier mode amplitudes, and the temporal behaviour of this quantity for various wavenumber pairs (n_x, n_z) is studied. Approximately periodic dynamics are found for certain (dominant) modal velocities; in particular, $\mathrm{M}(0,1)$ and $\mathrm{M}(1,0)$ remain in near antiphase: peaks (toughs) in the former often being accompanied troughs (peaks) in the latter: Fig. 2 (cf. Fig. 3(a) of HKW). This figure also shows that the temporal dynamics of $\mathrm{M}(1,1)$ is much the same as that of $\mathrm{M}(1,0)$, with a recurrence period is 80-100 nondimensional time units, while $\mathrm{M}(0,2)$ is less regular.

Fig. 3 (cf. Fig. 2 of HKW) shows mid-plane contours of the streamwise velocity at the times 1-8 noted on the $\mathrm{M}(0,1)$ curve in Fig. 2. At 1, the flow shows prominent streaks. The flow pattern then develops greater variation with respect to streamwise position, until at 5 the streaks break down. They then regenerate and at 8 the process begins anew. We show average streamwise velocity contours and cross-stream velocity vectors in the cross-stream plane in Fig. 4. To simplify the representation of these quantities we consider contributions from the streamwise-invariant modes only (cf. Fig. 4 of HKW). Here "before" and "after" breakdown correspond to the points 1 and 5 in Fig. 2). This plot shows that the contours of streamwise velocity are much the same after breakdown as before, with the contours being perhaps a little more diffuse. We also note that the cross-stream velocities increase during the breakdown process, as explained in HKW.

The streamwise velocity contours presented in Fig. 4 include the laminar solution $\mathbf{U}_0$. Versions of this plot in which the laminar solution is excluded are subsequently given in comparing these results with those of low-dimensional models.

2.3. *The proper orthogonal decomposition*

Numerous accounts of the POD are available, notably those of Sirovich (1987); Berkooz *et al.* (1993) and Holmes *et al.* (1996); rather than sketching the procedure again, we refer the reader to them and to our earlier paper on PCF (Moehlis *et al.* (2002)). We merely recall that the POD modes are the eigenfunctions of the integral operator equation

$$\sum_{j=1}^{3} \int\int\int_{\Omega} \langle u_i(\mathbf{x}, t) u_j^*(\mathbf{x}', t) \rangle \Phi_j^{(n)}(\mathbf{x}') d^3\mathbf{x}' = \lambda_{n_x, n_z}^{(n)} \Phi_i^{(n)}(\mathbf{x}), \tag{2.2}$$

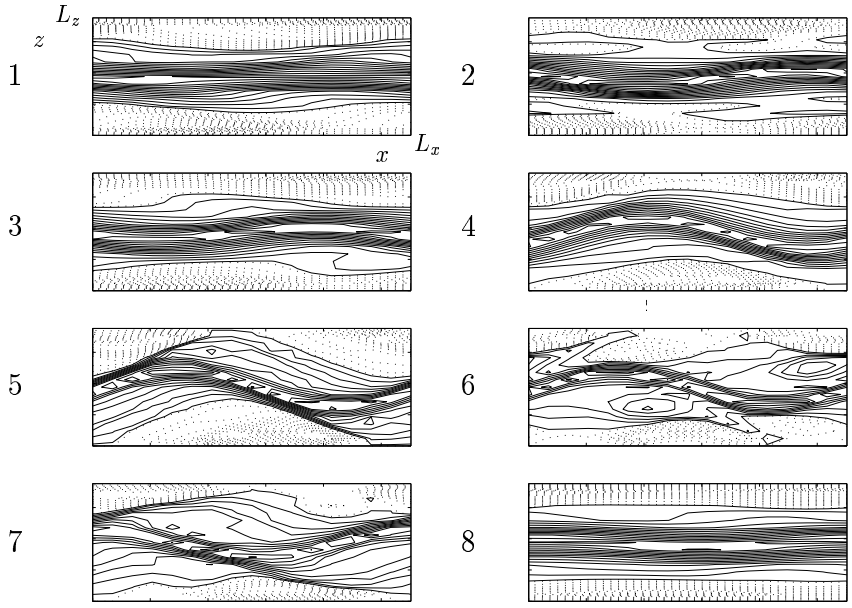

FIGURE 3. The streak breakdown process in DNS simulations of PCF in the MFU as indicated by contours of u (solid positive, dashed negative) in the (x, z) plane lying between the two plates. Here, and for similar plots in this paper, we label the axes in the subplot in the upper left-hand corner only. Since the laminar solution is identically zero in this mid-plane it makes no contribution to the contours in this plot.

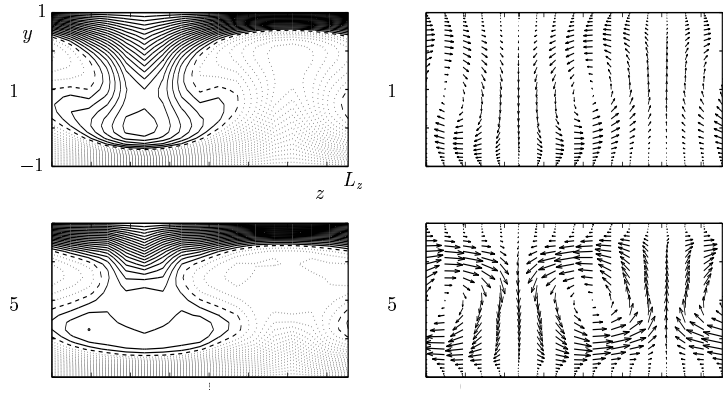

FIGURE 4. Streamwise velocity contours (left) and cross-stream velocity vectors (right) associated with streamwise-invariant modes before breakdown 1 and after breakdown 5.

where Ω denotes the flow domain, $\langle u_i(\mathbf{x},t)u_j^*(\mathbf{x}',t)\rangle$ the ensemble averaged autocorrelation tensor, and $\mathbf{\Phi}^{(n)} = (\Phi_1^{(n)}, \Phi_2^{(n)}, \Phi_3^{(n)})$ the POD modes, indexed by "quantum numbers" $n \in Z^+$ and streamwise and spanwise wavenumbers n_x, n_z. Translation invariance (1.7) implies that Fourier decompositions in the latter directions are optimal (Holmes *et al.* (1996)), and hence that we may write

$$\mathbf{\Phi}^{(n)}(\mathbf{x}) = \sum_{n_x,n_z} \mathbf{\Phi}^{(n)}_{n_x,n_z}(\mathbf{x}) = \frac{1}{\sqrt{L_x L_z}} \sum_{n_x,n_z} \exp\left(2\pi i\left(\frac{n_x x}{L_x} + \frac{n_z z}{L_z}\right)\right) \boldsymbol{\phi}^{(n)}_{n_x,n_z}(y). \quad (2.3)$$

The representation of the velocity field is therefore

$$\mathbf{u}(\mathbf{x},t) = \frac{1}{\sqrt{L_x L_z}} \sum_n \sum_{n_x} \sum_{n_z} a^{(n)}_{n_x,n_z}(t) \exp\left(2\pi i \left(\frac{n_x x}{L_x} + \frac{n_z z}{L_z}\right)\right) \boldsymbol{\phi}^{(n)}_{n_x,n_z}(y). \tag{2.4}$$

The modal coefficients $a^{(n)}_{n_x,n_z}$ are complex unless $n_x = n_z = 0$. However, reality of $\mathbf{u}$ and $\mathbf{\Phi}^{(n)}(\mathbf{x})$ implies

$$a^{(n)}_{n_x,n_z}(t) = a^{(n)*}_{-n_x,-n_z}(t) \text{ and } \boldsymbol{\phi}^{(n)}_{n_x,n_z}(y) = \boldsymbol{\phi}^{(n)*}_{-n_x,-n_z}(y). \tag{2.5}$$

We shall refer to $\boldsymbol{\phi}^{(n)}_{n_x,n_z}(y)$ as the (n,n_x,n_z) POD mode.

The eigenvalues $\lambda^{(n)}_{n_x,n_z}$ are equal to twice the average kinetic energy of the corresponding modes; thus their decay properties provide an indication of which modes should be included on energetic grounds.

As shown in Smith (2003); Moehlis *et al.* (2002), following the action of the discrete symmetries (1.4-1.6) through Fourier transformation and the POD, we deduce that the modal components behave as follows under the group elements:

$$\mathcal{P}\cdot\begin{pmatrix} \phi^{(n)}_{1,n_x,n_z}(y) \\ \phi^{(n)}_{2,n_x,n_z}(y) \\ \phi^{(n)}_{3,n_x,n_z}(y) \end{pmatrix} = \begin{pmatrix} -\phi^{(n)}_{1-n_x-n_z}(-y) \\ -\phi^{(n)}_{2-n_x-n_z}(-y) \\ -\phi^{(n)}_{3-n_x-n_z}(-y) \end{pmatrix}, \tag{2.6}$$

$$\mathcal{R}\cdot\begin{pmatrix} \phi^{(n)}_{1,n_x,n_z}(y) \\ \phi^{(n)}_{2,n_x,n_z}(y) \\ \phi^{(n)}_{3,n_x,n_z}(y) \end{pmatrix} = \begin{pmatrix} \phi^{(n)}_{1n_x-n_z}(y) \\ \phi^{(n)}_{2n_x-n_z}(y) \\ -\phi^{(n)}_{3n_x-n_z}(y) \end{pmatrix}, \tag{2.7}$$

$$\mathcal{R}\mathcal{P}\cdot\begin{pmatrix} \phi^{(n)}_{1,n_x,n_z}(y) \\ \phi^{(n)}_{2,n_x,n_z}(y) \\ \phi^{(n)}_{3,n_x,n_z}(y) \end{pmatrix} = \begin{pmatrix} -\phi^{(n)}_{1-n_x,n_z}(-y) \\ -\phi^{(n)}_{2-n_x,n_z}(-y) \\ \phi^{(n)}_{3-n_x,n_z}(-y) \end{pmatrix}. \tag{2.8}$$

A lengthy analysis, detailed in Smith (2003), then allows us to deduce the following actions of $\mathcal{P}$ and $\mathcal{R}$ on the modal amplitude coefficients $a^{(n)}_{n_x,n_z}$:

$$\mathcal{P}\cdot a^{(n)}_{n_x,n_z}(t) = c_{\mathcal{P}} a^{(n)}_{-n_x,-n_z}(t), \tag{2.9}$$

$$\mathcal{R}\cdot a^{(n)}_{n_x,n_z}(t) = c_{\mathcal{R}} a^{(n)}_{n_x,-n_z}(t), \tag{2.10}$$

$$\mathcal{R}\mathcal{P}\cdot a^{(n)}_{n_x,n_z}(t) = c_{\mathcal{P}} c_{\mathcal{R}} a^{(n)}_{-n_x,n_z}(t), \tag{2.11}$$

where

$$c_{\mathcal{P}} = \begin{cases} -1 & \text{if } n_x = n_z = 0 \text{ and } \phi^{(n)}_{0,0} \text{ has components even in } y \\ +1 & \text{otherwise} \end{cases}, \tag{2.12}$$

$$c_{\mathcal{R}} = \begin{cases} -1 & \text{if } n_x = n_z = 0 \text{ and } \phi^{(n)}_{3,0,0} = 0 \\ -1 & \text{if } n_z = 0 \text{ and } \phi^{(n)}_{1,n_x,0} = \phi^{(n)}_{2,n_x,0} = 0 \\ +1 & \text{otherwise} \end{cases}. \tag{2.13}$$

Table 1 shows the eigenvalues associated with the first twelve (sets of) POD modes in order of decreasing eigenvalue magnitude. Here

$$\%E^{(n)}_{n_x,n_z} \stackrel{\text{def}}{=} \left(\lambda^{(n)}_{n_x,n_z} \Big/ \sum_{m,m_x,m_z} \lambda^{(m)}_{m_x,m_z}\right) \times 100$$

TABLE 1. Eigenvalues for the POD modes for PCF in the MFU.

(n, n_x, n_z)	$\lambda^{(n)}_{n_x,n_z}$	$\%E^{(n)}_{n_x,n_z}$
$(1,0,0)$	4.4550	68.02
$(1,0,\pm1)$	0.7821	23.88
$(1,0,\pm2)$	0.0543	1.66
$(1,\pm1,0)$	0.0386	1.18
$(1,0,\pm3)$	0.0195	0.59
$(2,0,0)$	0.0174	0.27
$(2,0,\pm1)$	0.0123	0.38
$(1,\pm1,\pm2)$	0.0109	0.33
$(1,\pm1,\pm1)$	0.0090	0.27
$(3,0,0)$	0.0068	0.10
$(4,0,0)$	0.0054	0.08
$(3,0,\pm1)$	0.0039	0.12
$\cdots$		

is the percentage of average total energy contained in the (n, n_x, n_z) POD mode. The symmetries guarantee that $\lambda^{(n)}_{n_x,n_z} = \lambda^{(n)}_{n_x,-n_z}$, and we lump these modes together accordingly. (Hence the $(2,0,\pm1)$ POD modes, each with eigenvalue of 0.0123, together account for more kinetic energy on average than the $(2,0,0)$ mode with eigenvalue 0.0174.)

The three most energetic modes have Fourier wavenumbers $(0,0)$, $(0,1)$, $(0,2)$; a similar triad appeared in the Moderate Aspect Ratio PCF study of Moehlis *et al.* (2002). Interestingly, the fourth most energetic mode is the spanwise-invariant $(1,1,0)$ mode, which has neither a streamwise nor a wall-normal component and is thus unable to directly interact with the $(1,0,0)$ mode representing the mean flow. In Fig. 5 we show the $(1,0,0)$ mode and indicate its close approximation to the full (DNS) mean velocity profile. The "two-dimensional modes" which follow the $(1,0,0)$ mode in Table 1 are plotted in Fig. 6. Over 90% of the turbulent kinetic energy is captured by the first two modes, while 99% is captured by the leading 43 modes. Table 1 agrees well with independent results of Gibson (2002).

3. Coupled low-dimensional models for the MFU

We first briefly describe the general derivation and some properties of the ODEs resulting from Galerkin projection of the Navier-Stokes equations onto subspaces spanned by sets of POD modes. Inserting (2.4) into (1.1) and performing a Galerkin projection, we obtain ODEs of the form

$$\dot{a}^{(n)}_{n_x,n_z} = \sum_{k=1}^{\infty} \hat{A}^{(n,k)}_{n_x,n_z} a^{(k)}_{n_x,n_z} + [N(\mathbf{a},\mathbf{a})]_{n,n_x,n_z}, \tag{3.1}$$

$$n = 1,2,\cdots, \quad n_x, n_z = \cdots,-2,-1,0,1,2,\cdots,$$

where

$$[N(\mathbf{a},\mathbf{a})]_{n,n_x,n_z} \stackrel{\text{def}}{=} \sum_{\substack{m,k,\\ m_x,m_z}} \hat{B}^{(n,m,k)}_{n_x,n_z m_x m_z} a^{(m)}_{m_x,m_z} a^{(k)}_{n_x-m_x,n_z-m_z},$$

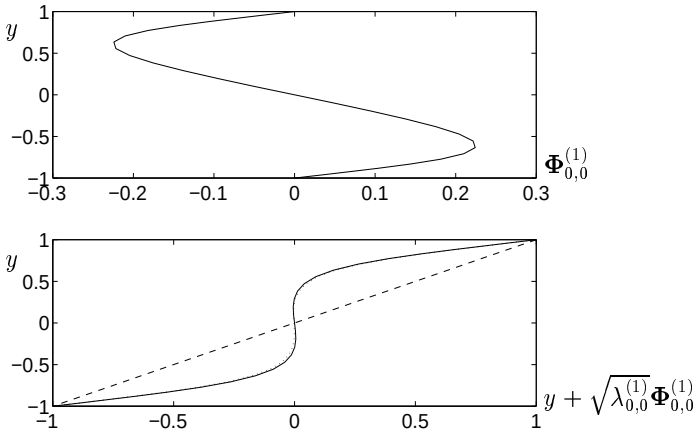

FIGURE 5. The x-component of the POD mode $\mathbf{\Phi}^{(1)}_{0,0}$ (top). The y and z-components are equal to zero. The velocity profile obtained by adding this POD mode with r.m.s. amplitude $\sqrt{\lambda^{(1)}_{0,0}} = \sqrt{\langle |a^{(1)}_{0,0}(t)|^2 \rangle}$ to the laminar state $\mathbf{U}_0 = z\mathbf{e}_x$ (bottom). The mean flow obtained from the full DNS ensemble average is also indicated (dotted curve, barely discernable).

and, letting $'$ denote differentiation with respect to z,

$$\begin{aligned}\hat{A}^{(n,k)}_{n_x,n_z} \stackrel{\text{def}}{=} & -\frac{1}{Re}\left(\left(\frac{2\pi n_x}{L_x}\right)^2 + \left(\frac{2\pi n_z}{L_z}\right)^2\right)\delta_{nk} \\ & - \int_{-1}^{1} \phi^{(n)}_{2,n_x,n_z}\phi^{(k)*}_{1,n_x,n_z}\,dy - \frac{2\pi i n_x}{L_x}\sum_{j=1}^{3}\int_{-1}^{1} y\phi^{(n)}_{j,n_x,n_z}\phi^{(k)*}_{j,n_x,n_z}\,dy \\ & - \frac{1}{Re}\sum_{j=1}^{3}\int_{-1}^{1}\phi^{(n)'}_{j,n_x,n_z}\phi^{(k)*'}_{j,n_x,n_z}\,dy, \end{aligned} \tag{3.2}$$

$$\begin{aligned}\hat{B}^{(n,m,k)}_{n_x,n_z m_x m_z} \stackrel{\text{def}}{=} & -\frac{1}{\sqrt{L_x L_z}}\sum_{j=1}^{3}\int_{-1}^{1}\left(\frac{2\pi i m_x}{L_x}\phi^{(k)}_{1,n_x-m_x,n_z-m_z}\phi^{(m)}_{jm_x m_z}\right. \\ & + \phi^{(k)}_{2,n_x-m_x,n_z-m_z}\phi^{(m)'}_{jm_x m_z} \\ & \left. + \frac{2\pi i m_z}{L_z}\phi^{(k)}_{3,n_x-m_x,n_z-m_z}\phi^{(m)}_{jm_x m_z}\right)\phi^{(n)*}_{j,n_x,n_z}\,dy. \end{aligned} \tag{3.3}$$

The projected ODEs (3.1) are equivariant with respect to the group actions (2.9-2.11) and the continuous symmetries

$$\mathcal{T}_{\Delta x} : a^{(n)}_{n_x,n_z}(t) \mapsto e^{in_x\phi_x}a^{(n)}_{n_x,n_z}(t), \tag{3.4}$$

$$\mathcal{T}_{\Delta z} : a^{(n)}_{n_x,n_z}(t) \mapsto e^{in_z\phi_z}a^{(n)}_{n_x,n_z}(t), \tag{3.5}$$

where $\phi_x = 2\pi\Delta x/L_x$ and $\phi_z = 2\pi\Delta z/L_z$; i.e., writing (3.1) as $\dot{\mathbf{a}} = f(\mathbf{a})$, it is necessary that $f(\gamma\mathbf{a}) = \gamma f(\mathbf{a})$ for all $\gamma \in O(2)\times O(2)$. This implies that many terms which might appear in (3.1), in fact, vanish. Also, by exploiting symmetry properties of the POD modes (specifically, oddness or evenness of components $\phi^{(n)}_{i,n_x,n_z}$ under $y \to -y$), it can be shown that certain of the $\hat{A}$'s and $\hat{B}$'s vanish identically. Finally, the nonlinear terms

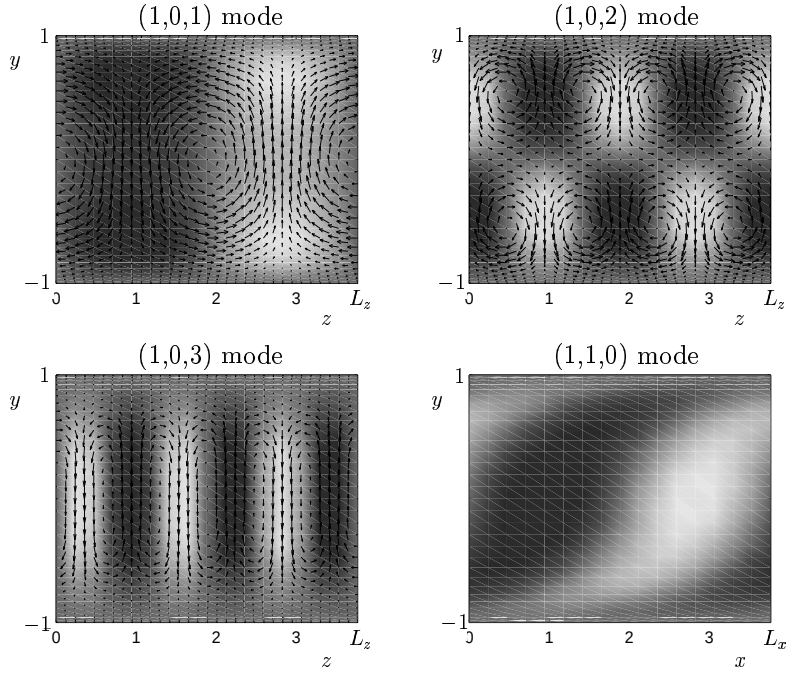

FIGURE 6. Flow fields $\mathbf{u}$ associated with the $(n, n_x, n_z) = (1, 0, 1)$, $(1, 0, 2)$, $(1, 0, 3)$ and $(1, 1, 0)$ POD modes. For the $(1, 0, 1)$, $(1, 0, 2)$ and $(1, 0, 3)$ POD modes the vectors show the spanwise and wall-normal velocities, while the dark (light) shading denotes positive (negative) streamwise velocity. For the $(1, 1, 0)$ mode the u and v components are identically zero, and the dark (light) shading now denotes positive (negative) *spanwise* velocity.

in the Navier-Stokes equations are energy-conserving. Specifically, we have

$$\begin{aligned}\int\int\int_\Omega \mathbf{u}\cdot(\mathbf{u}\cdot\nabla\mathbf{u})d^3\mathbf{x} &= \int\int\int_\Omega \mathbf{u}\cdot\left(\nabla\left(\frac{1}{2}\mathbf{u}\cdot\mathbf{u}\right)-\mathbf{u}\times(\nabla\times\mathbf{u})\right)d^3\mathbf{x}\\ &= \int\int\int_\Omega \nabla\cdot\left(\left(\frac{1}{2}\mathbf{u}\cdot\mathbf{u}\right)\mathbf{u}\right)d^3\mathbf{x}\\ &= \int\int_{\partial\Omega}\left(\frac{1}{2}\mathbf{u}\cdot\mathbf{u}\right)\mathbf{u}\cdot\hat{\mathbf{n}}\,dS = 0,\end{aligned} \tag{3.6}$$

where we have used vector identities, the facts that $\mathbf{u}\cdot(\mathbf{u}\times(\nabla\times\mathbf{u})) = 0$ and $\nabla\cdot\mathbf{u} = 0$, and the divergence theorem. The surface integral vanishes due to the no-slip boundary conditions at $z = \pm 1$ and periodicity in the x and z-directions. Using (2.4), it can be shown that Eqn. (3.6) is equivalent to

$$\sum_{n=1}^{\infty}\sum_{n_x=-\infty}^{\infty}\sum_{n_z=-\infty}^{\infty} a^{(n)*}_{n_x,n_z}[N(\mathbf{a},\mathbf{a})]_{n,n_x,n_z} = 0. \tag{3.7}$$

Eqn. (3.7) and the symmetries (2.9-2.11) and (3.4-3.5) provide checks on the numerically computed nonlinear coefficients: in all cases we have found that (3.7) is satisfied to 0.01%, and we have therefore subsequently rounded off the coefficients to ensure that these symmetries are exactly respected.

In Smith (2003) the implications of the symmetries inherent in (2.6-2.11) are developed for the specific truncations considered below. This allows one to identify numerous (nested) invariant subspaces, much as for the wall layer model of Aubry *et al.* (1988),

cf. Holmes *et al.* (1996). We shall only draw on small parts of this analysis below, so largely omit it here and in §4.

The ODEs (3.1) are similar to those of the turbulent boundary layer problem in Aubry *et al.* (1988), with the following important differences. In Aubry *et al.* (1988), in place of $\mathbf{U}_0 = y\mathbf{e}_x$, the analog of (1.1) involves a spatially-averaged (t-dependent) mean turbulent velocity, modeled as a balance between the effects of pressure and those of the coherent structures, giving cubic terms in the ODEs. No such modeling is required here: the nonlinear terms derive directly from (1.1) and the $n_x = n_z = 0$ modes represent time-varying turbulent modifications to the mean. Second, the contribution from the pressure term at the outer edge of the wall layer was modeled as stochastic forcing in Aubry *et al.* (1988); here, it makes no contribution because of the divergence-free expansion (2.4) and no-slip and periodic conditions at the boundaries of Ω Holmes *et al.* (1996). Finally, in Aubry *et al.* (1988) the ODEs are equivariant under $O(2) \times S^1$; here, the additional reflection and rotation symmetries make the ODEs equivariant under $O(2)\times O(2)$, further constraining the modal interactions.

3.1. *High-dimensional truncations*

While we are primarily interested in deriving (very) low-dimensional models by the POD-Galerkin procedure, it is of interest first to determine how relatively *large* truncations capture the detailed dynamics of the DNS database, as in Moehlis *et al.* (2002). To this end, in Fig. 7 we present numerical simulations of a model containing the 600 most energetic POD modes. This achieves good short-term tracking for ≈ 20 non-dimensional time units, after which sensitive dependence on initial conditions inevitably drives the model and DNS trajectories apart, although the long term statistics of the 12 most energetic modes are reproduced well. In the lower panels of Fig. 7 (cf. Figs. 8 and 13, below) we show projections of the model and DNS solutions onto the two most energetic modes $(1,0,\pm1), (1,0,\pm2)$ following the mean $(1,0,0)$, illustrating that the model modes display similar behaviour to the DNS modes, with occasional (unphysical) excursions to the trivial state, corresponding to near-relaminarisation of the flow. We note that this effect disappears once ≈ 1000 modes are retained.

John Gibson, who independently studied the same problem in Gibson (2002), also determined that approximately 1000 modes were required to faithfully reproduce the DNS behaviour.

3.2. *Structure of the projected ODEs*

3.2.1. *The coupled 9-mode model: dynamical equations*

We first display the equations resulting from a projection which includes all $n = 1$ modes in Table 1 ($(1,0,0)$, $(1,0,1)$, $(1,0,2)$, $(1,1,0)$, $(1,1,\pm1)$, $(1,0,3)$, and $(1,1,\pm2)$). This will encompass all the models considered in this section. Here the ODEs (3.1) take the particular form:

$$\begin{aligned}
\dot{a}^{(1)}_{0,0} &= A_{0,0}\; a^{(1)}_{0,0} + 2(B_{0,1}|a^{(1)}_{0,1}|^2 + B_{0,2}|a^{(1)}_{0,2}|^2 + B_{0,3}|a^{(1)}_{0,3}|^2 \\
&+ B_{1,1}(|a^{(1)}_{1,1}|^2 + |a^{(1)}_{1,-1}|^2) + B_{1,2}(|a^{(1)}_{1,2}|^2 + |a^{(1)}_{1,-2}|^2)),
\end{aligned}$$

$$\begin{aligned}
\dot{a}^{(1)}_{0,1} &= (A_{0,1} - B_{0,1}a^{(1)}_{0,0})\; a^{(1)}_{0,1} \\
&- {}^{0,1}C^{0,2}_{0,1}a^{(1)}_{0,2}a^{(1)*}_{0,1} + ({}^{0,1}C^{1,0}_{1,-1} - {}^{0,1}C^{1,1}_{1,0})a^{(1)}_{1,1}a^{(1)*}_{1,0} \\
&- ({}^{0,1}C^{1,-1}_{1,-2} + {}^{0,1}C^{1,2}_{1,1})a^{(1)}_{1,-1}a^{(1)*}_{1,-2} - ({}^{0,1}C^{0,3}_{0,2} + {}^{0,1}C^{0,-2}_{0,-3})a^{(1)}_{0,3}a^{(1)*}_{0,2} \\
&+ ({}^{0,1}C^{1,2}_{1,1} + {}^{0,1}C^{1,-1}_{1,-2})a^{(1)}_{1,2}a^{(1)*}_{1,1} + ({}^{0,1}C^{1,1}_{1,0} - {}^{0,1}C^{1,0}_{1,-1})a^{(1)}_{1,0}a^{(1)*}_{1,-1}
\end{aligned}$$

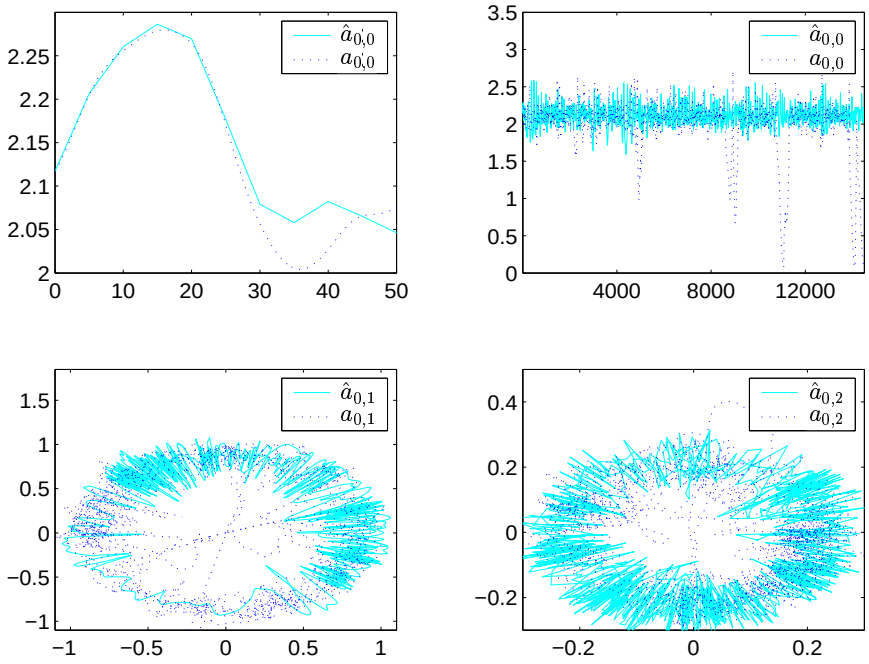

FIGURE 7. Short term tracking and phase space geometry for a high-dimensional POD-based model of plane Couette flow (PCF). Top panels: short and long time histories of $(1,0,0)$ "mean flow" modes for DNS (solid) and model (dashed). Bottom panels: projections of DNS (solid) and model (dashed) solutions onto the complex $(1,0,\pm 1)$ and $(1,0,\pm 2)$ modal planes. . In this figure, and similar ones that follow, the superscript (1) has been dropped from the lablels for clarity.

$$
\begin{aligned}
\dot{a}^{(1)}_{0,2} &= (A_{0,2} - B_{0,2}a^{(1)}_{0,0})\, a^{(1)}_{0,2} \\
&- ({}^{0,2}C^{1,0}_{1,-2} + {}^{0,2}C^{1,2}_{1,0})a^{(1)}_{1,0}a^{(1)*}_{1,-2} + {}^{0,1}C^{0,2}_{0,1}(a^{(1)}_{0,1})^2 - 2\,{}^{0,2}C^{1,1}_{1,-1}a^{(1)}_{1,1}a^{(1)}_{1,-1} \\
&+ ({}^{0,1}C^{0,-2}_{0,-3} - {}^{0,2}C^{0,3}_{0,1})a^{(1)}_{0,3}a^{(1)}_{0,-1} - ({}^{0,2}C^{1,2}_{1,0} + {}^{0,2}C^{1,0}_{1,-2})a^{(1)}_{1,2}a^{(1)}_{-1,0}
\end{aligned}
$$

$$
\begin{aligned}
\dot{a}^{(1)}_{1,0} &= A_{1,0}\, a^{(1)}_{1,0} \\
&+ ({}^{0,1}C^{1,0}_{1,-1} - {}^{1,0}C^{1,-1}_{0,1})a^{(1)}_{0,1}a^{(1)}_{1,-1} + ({}^{0,2}C^{1,0}_{1,-2} + {}^{1,0}C^{1,-2}_{0,2})a^{(1)}_{0,2}a^{(1)}_{1,-2} \\
&+ ({}^{1,0}C^{1,-1}_{0,1} - {}^{0,1}C^{1,0}_{1,-1})a^{(1)}_{1,1}a^{(1)*}_{0,1} + ({}^{1,0}C^{1,-2}_{0,2} + {}^{0,2}C^{1,0}_{1,-2})a^{(1)}_{1,2}a^{(1)*}_{0,2}
\end{aligned}
$$

$$
\begin{aligned}
\dot{a}^{(1)}_{1,1} &= (A_{1,1} - B_{1,1}a^{(1)}_{0,0})\, a^{(1)}_{1,1} \\
&+ ({}^{0,1}C^{1,1}_{1,0} - {}^{1,0}C^{1,-1}_{0,1})a^{(1)}_{0,1}a^{(1)}_{1,0} + {}^{0,1}C^{0,3}_{0,2}a^{(1)}_{0,2}a^{(1)}_{1,-1} \\
&+ ({}^{1,1}C^{1,-2}_{0,-3} + {}^{1,1}C^{0,3}_{-1,2})a^{(1)}_{0,3}a^{(1)}_{1,-2} - ({}^{1,1}C^{1,2}_{0,1} + {}^{0,1}C^{1,-1}_{1,-2})a^{(1)}_{1,2}a^{(1)}_{0,-1}
\end{aligned}
$$

$$
\begin{aligned}
\dot{a}^{(1)}_{1,-1} &= (A_{1,1} - B_{1,1}a^{(1)}_{0,0})\, a^{(1)}_{1,-1} \\
&+ ({}^{0,1}C^{1,-1}_{1,-2} + {}^{1,1}C^{1,2}_{0,1})a^{(1)}_{0,1}a^{(1)}_{1,-2} + {}^{0,1}C^{0,3}_{0,2}a^{(1)}_{0,-2}a^{(1)}_{1,1} \\
&+ ({}^{1,0}C^{1,-1}_{0,1} - {}^{0,1}C^{1,1}_{1,0})a^{(1)}_{1,0}a^{(1)}_{0,-1} - ({}^{1,1}C^{0,3}_{-1,2} + {}^{1,1}C^{1,-2}_{0,-3})a^{(1)}_{1,2}a^{(1)}_{0,-3}
\end{aligned}
$$

$$
\begin{aligned}
\dot{a}^{(1)}_{0,3} &= (A_{0,3} - B_{0,3}a^{(1)}_{0,0})\, a^{(1)}_{0,3} \\
&+ ({}^{0,1}C^{0,3}_{0,2} + {}^{0,2}C^{0,3}_{0,1})a^{(1)}_{0,1}a^{(1)}_{0,2} + ({}^{0,3}C^{1,2}_{1,-1} - {}^{1,1}C^{1,-2}_{0,-3})a^{(1)}_{1,1}a^{(1)}_{-1,2} \\
&+ ({}^{1,1}C^{1,-2}_{0,-3} - {}^{0,3}C^{1,2}_{1,-1})a^{(1)}_{-1,1}a^{(1)}_{1,2}
\end{aligned}
$$

TABLE 2. Coefficients for the system (3.8).

n_x	n_z	A'_{n_x,n_z}	A''_{n_x,n_z}	B_{n_x,n_z}
0	0	0	10.7603	0
0	1	0.1281	9.8256	0.0386
0	2	-0.0503	21.8841	-0.0074
1	0	0	9.9411	0
1	1	0.0141	14.9003	0.0006
0	3	-0.0562	27.9672	-0.0226
1	2	0.2430	18.3647	0.0876

$$\begin{aligned}
\dot{a}^{(1)}_{1,2} &= (A_{1,2} - B_{1,2}a^{(1)}_{0,0})\, a^{(1)}_{1,2} + ({}^{1,1}C^{1,2}_{0,1} - {}^{0,1}C^{1,2}_{1,1})a^{(1)}_{0,1}a^{(1)}_{1,1} \\
&+ ({}^{0,2}C^{1,2}_{1,0} - {}^{1,0}C^{1,-2}_{0,2})a^{(1)}_{1,0}a^{(1)}_{0,2} + ({}^{1,1}C^{0,3}_{-1,2} + {}^{0,3}C^{1,2}_{1,-1})a^{(1)}_{0,3}a^{(1)}_{1,-1} \\
\dot{a}^{(1)}_{1,-2} &= (A_{1,2} - B_{1,2}a^{(1)}_{0,0})\, a^{(1)}_{1,-2} + ({}^{0,2}C^{1,2}_{1,0} - {}^{1,0}C^{1,-2}_{0,2})a^{(1)}_{1,0}a^{(1)}_{0,-2} \\
&- ({}^{1,1}C^{0,3}_{-1,2} + {}^{0,3}C^{1,2}_{1,-1})a^{(1)}_{1,1}a^{(1)}_{0,-3} + ({}^{0,1}C^{1,2}_{1,1} - {}^{1,1}C^{1,2}_{0,1})a^{(1)}_{1,-1}a^{(1)}_{0,-1}
\end{aligned} \tag{3.8}$$

where the A_{n_x,n_z} may be partitioned as

$$A_{n_x,n_z} \stackrel{\text{def}}{=} A'_{n_x,n_z} - A''_{n_x,n_z}/Re, \tag{3.9}$$

with A'_{n_x,n_z}'s, A''_{n_x,n_z}'s and B_{n_x,n_z}'s given in Table 2, and the remaining nonlinear terms as follows:

$${}^{0,1}C^{0,2}_{0,1} = 0.0647, \quad {}^{0,1}C^{1,0}_{1,-1} = 0.0120, \quad {}^{0,1}C^{1,1}_{1,0} = 0.1833, \quad {}^{0,1}C^{1,-1}_{1,-2} = 0.0445,$$

$${}^{0,1}C^{1,2}_{1,1} = 0.1199, \quad {}^{0,1}C^{0,-2}_{0,-3} = 0.0002, \quad {}^{0,1}C^{0,3}_{0,2} = 0.0006, \quad {}^{0,2}C^{1,0}_{1,-2} = 0.0074,$$

$${}^{0,2}C^{1,2}_{1,0} = 0.2374, \quad {}^{0,2}C^{1,-1}_{1,1} = 0.0595, \quad {}^{0,2}C^{0,3}_{0,1} = 0.1517, \quad {}^{1,0}C^{1,-1}_{0,1} = 0.0828,$$

$${}^{1,0}C^{1,-2}_{0,2} = 0.0083, \quad {}^{1,1}C^{1,-2}_{0,-3} = 0.2413, \quad {}^{1,1}C^{0,3}_{-1,2} = 0.1171,$$

$${}^{1,1}C^{1,2}_{0,1} = 0.1723, \quad {}^{0,3}C^{1,2}_{1,-1} = 0.346786.$$

The nine modes included in this model capture 95.9% of the kinetic energy on average, and the equations describe a 17-dimensional dynamical system (recall that all but the $n_x = n_z = 0$ modal amplitude coefficients are complex, and that for those triads with two nonzero Fourier wavenumbers, two independent coefficients must be allowed). The laminar ($a^{(1)}_{n_x,n_z} = 0$) state for this model (without modeling losses as in §3.3) is unstable at sufficiently large Reynolds numbers due to the linear coefficients of the $(1,0,1)$, $(1,1,\pm1)$ and $(1,1,\pm2)$ modes. The first and last two of these three modes span an invariant subspace, although this is an artefact of the truncation that does not, e.g., survive addition of the $(1,0,4)$ mode.

3.2.2. *Preliminary comments on choice of modal groups*

Since the first four modes of Table 1 capture 94.7% of the average turbulent kinetic energy, it seems reasonable to base a model on these four, adding other modes necessary to retain appropriate Fourier wavenumber interactions. This leads us to consider an 11-dimensional model based on the six modes ($(1,0,0)$, $(1,0,1)$, $(1,0,2)$, $(1,1,0)$ and $(1,1,\pm1)$), the equations for which may be obtained by setting $a^{(1)}_{0,3} = a^{(1)}_{1,\pm2} = 0$ in

the first six equations of the system (3.8) and dropping the equations for the omitted variables.

We also note that the interaction among the $(1,0,0)$, $(1,0,1)$ and $(1,0,2)$ modes, which together capture 93.5% the most turbulent kinetic energy on average according to Table 1, is determined by the following three, relatively simple, ODEs:

$$\begin{aligned} \dot{a}_{0,0}^{(1)} &= A_{0,0}\ a_{0,0}^{(1)} + 2(B_{0,1}|a_{0,1}^{(1)}|^2 + B_{0,2}|a_{0,2}^{(1)}|^2), \\ \dot{a}_{0,1}^{(1)} &= (A_{0,1} - B_{0,1}a_{0,0}^{(1)})\ a_{0,1}^{(1)} - {}^{0,1}C_{0,1}^{0,2} a_{0,2}^{(1)} a_{0,1}^{(1)*}, \\ \dot{a}_{0,2}^{(1)} &= (A_{0,2} - B_{0,2}a_{0,0}^{(1)})\ a_{0,2}^{(1)} + {}^{0,1}C_{0,1}^{0,2}(a_{0,1}^{(1)})^2. \end{aligned} \tag{3.10}$$

This minimal model is the "energy-conserving" quadratic normal form of the 0:1:2 resonance. While it does not reproduce the turbulent dynamics accurately, it does form an analytically tractable "core" of larger models such as (3.8), and we shall perform a detailed analysis of it elsewhere (Smith *et al.* (2004)).

3.3. *Modelling neglected modes*

Before considering the dynamics of the six- and nine-mode models we describe a crude model for capturing interactions with modes neglected in these truncations. Henceforth we denote the "true" modal amplitude obtained by projection of the DNS data onto the (n, n_x, n_z) mode by $\hat{a}_{n_x,n_z}^{(n)}$. We follow Podvin & Lumley (1998); Podvin (2001) and calculate, for each of these true modal amplitudes, the effect of the neglected modes on the POD mode under consideration, given by

$$\widehat{T}_{n_x,n_z}^{(n)} = \sum_{n' \neq n} A_{n_x n_y}^{(n',n)} \hat{a}_{n_x,n_z}^{(n')} + \sum B_{n_x n_z m_x m_z}^{(n,m,k)} \hat{a}_{m_x,m_z}^{(m)} \hat{a}_{n_x-m_x,n_z-m_z}^{(k)}. \tag{3.11}$$

Here the the first sum is over all n' such that (n', n_x, n_z) is not in the truncation, while the second sum is over all m, k, m_x, m_z such that (m, m_x, m_z) and $(k, n_x - m_x, n_z - m_z)$ are not in the truncation.

Having calculated this quantity, we determine how well it correlates with the corresponding coefficient $\hat{a}_{n_x,n_z}^{(n)}$. We define the scalar product between two complex-valued functions of time $f(t)$ and $g(t)$ as

$$\langle f|g\rangle \stackrel{\text{def}}{=} \lim_{t\to\infty} \int_0^t f(s)g^*(s)ds, \tag{3.12}$$

with the associated norm

$$\|f\| \stackrel{\text{def}}{=} \langle f|f\rangle^{1/2}. \tag{3.13}$$

The correlation coefficient between $f(t)$ and $g(t)$ is then defined to be

$$C(f,g) \stackrel{\text{def}}{=} \frac{\mathcal{R}[\langle f|g\rangle]}{(\langle f|f\rangle\langle g|g\rangle)^{1/2}}. \tag{3.14}$$

If $\widehat{T}_{n_x,n_z}^{(n)}$ and $\hat{a}_{n_x,n_z}^{(n)}$ are significantly anti-correlated ($-C > 0.5$, say), we may employ the linear approximation

$$\widehat{T}_{n_x,n_z}^{(n)} \approx -\beta_{n_x,n_z}^{(n)} \hat{a}_{n_x,n_z}^{(n)};\ \ \beta_{n_x,n_z}^{(n)} > 0, \tag{3.15}$$

which allows closure of the truncated system by approximating $\widehat{T}_{n_x,n_z}^{(n)}$ by an additional damping term:

$$\dot{a}_{n_x,n_z}^{(n)} = \text{terms from truncation} - \beta_{n_x,n_z}^{(n)} a_{n_x,n_z}^{(n)}. \tag{3.16}$$

The error induced in (3.15),

$$\begin{aligned}&\|\widehat{T}^{(n)}_{n_x,n_z} + \beta^{(n)}_{n_x,n_z}\hat{a}^{(n)}_{n_x,n_z}\|^2\\ &= \int_0^t (\widehat{T}^{(n)}_{n_x,n_z} + \beta^{(n)}_{n_x,n_z}\hat{a}^{(n)}_{n_x,n_z})(\widehat{T}^{(n)*}_{n_x,n_z} + \beta^{(n)}_{n_x,n_z}\hat{a}^{(n)*}_{n_x,n_z})\ dt,\end{aligned}$$

can be minimized in a least squares sense by setting

$$\beta^{(n)}_{n_x,n_z} \stackrel{\text{def}}{=} -\frac{\int_0^t (\widehat{T}^{(n)}_{n_x,n_z}\hat{a}^{(n)*}_{n_x,n_z} + \hat{a}^{(n)}_{n_x,n_z}\widehat{T}^{(n)*}_{n_x,n_z})\ dt}{2\int_0^t |\hat{a}^{(n)}_{n_x,n_z}|^2\ dt}, \tag{3.17}$$

which reveals the optimal damping required for each mode.

Applying this below we find that the correlation coefficients $C(\widehat{T}^{(n)}_{n_x,n_z}, \hat{a}^{(n)}_{n_x,n_z})$ vary considerably and the approximation (3.15) is thus more convincing for some modes than others. We shall attempt to reduce the effects of this variability by lumping the damping coefficients $\beta^{(n)}_{n_x,n_z}$ into a single model-specific damping coefficient via the weighted average over all modes contained in the model:

$$\nu \stackrel{\text{def}}{=} \left\langle \beta^{(n)}_{n_x,n_z}/(n_x^2+n_z^2) \right\rangle. \tag{3.18}$$

Losses to each mode will then be approximated as

$$\widehat{T}^{(n)}_{n_x,n_z} \approx -\alpha\nu(n_x^2+n_z^2)a^{(n)}_{n_x,n_z}, \tag{3.19}$$

where $\alpha = 1$ corresponds to a standard spectral eddy viscosity model (c.f Pope (2000), p. 610).

Eqn. (3.19) implies that $\widehat{T}^{(n)}_{0,0}$ is identically zero, and thus no attempt is made to model the influence of the neglected terms on the $(1,0,0)$ mode. This "mean flow" mode is problematic since first, for all truncations considered, $\widehat{T}^{(1)}_{0,0}$ oscillates about a mean close to zero, whilst the mean of $a^{(1)}_{0,0}$ hovers around 2.1. It is thus no simple matter to approximate $\widehat{T}^{(1)}_{0,0}$ with a function of the form $-\beta a^{(1)}_{0,0}$. Secondly, plots of $\widehat{T}^{(1)}_{0,0}$ amply demonstrate the fact that the $a^{(1)}_{0,0}$ mode is often subject to backscatter: energy flows from the neglected modes back to this mode. Indeed, the first equation of (3.8) indicates that energy flows from the $(1,n_x,n_z)$ mode into the $(1,0,0)$ mode whenever B_{n_x,n_z} is positive, and this is a primary mechanism sustaining nontrivial behaviour identified in Moehlis *et al.* (2002)

In carrying out the average (3.18) we reduce the (bifurcation) parameters to two: namely, the Reynolds number Re and α, an $\mathcal{O}(1)$ parameter adjusting the losses to the neglected modes.

3.4. *Dynamical behaviour of the coupled models*

3.4.1. *The 6-mode model*

We now consider the dynamics of the coupled 6-mode model, constructed from a Galerkin projection of (1.1) onto the $(1,0,0)$, $(1,0,1)$, $(1,0,2)$, $(1,1,0)$, $(1,1,\pm1)$ modes. Here and throughout §3, all computations are done at at $Re = 400$. Integration of this 11-dimensional dynamical system, without modelling losses to neglected modes, reveals travelling waves of the form

$$a^{(n)}_{n_x,n_z} = r^{(n)}_{n_x,n_z}\exp(i(-\omega n_z t + \alpha^{(n)}_{n_x,n_z})), \tag{3.20}$$

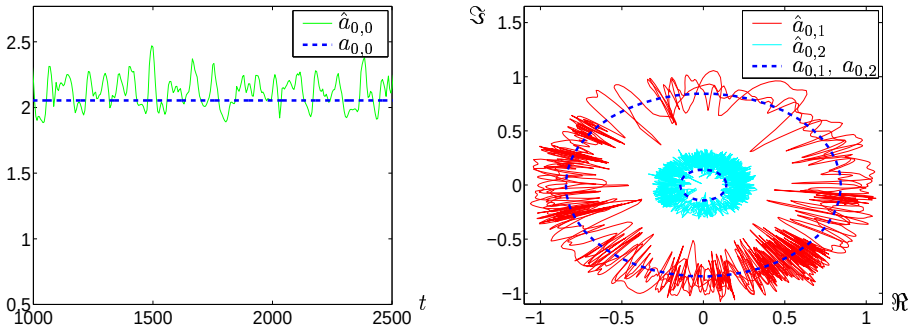

FIGURE 8. Behaviour of the coupled 6-mode model compared to the DNS projected onto the $(1,0,0)$, $(1,0,1)$ and $(1,0,2)$ modes. Here each of $a_{0,0}$, $a_{0,1}$, $a_{0,2}$ are shown as dashed lines, and are intended to represent approximations to the nearest (noisy) $\hat{a}_{n_x,n_z}$ line.

TABLE 3. Mean behaviour of the undamped coupled 6-mode model.

(n, n_x, n_y)	$\lambda^{(n)}_{n_x,n_z}$	$(r^{(n)}_{n_x,n_z})^2$
$(1,0,0)$	4.4550	4.2171
$(1,0,\pm1)$	0.7821	0.7134
$(1,0,\pm2)$	0.0543	0.0202
$(1,\pm1,0)$	0.0386	0.2791
$(1,\pm1,\pm1)$	0.0090	0.1752

where the reality of $a^{(1)}_{0,0}$ requires that $\alpha^{(1)}_{0,0}$ is necessarily zero. The amplitudes of the $(1,0,0)$, $(1,0,1)$ and $(1,0,2)$ modes are plotted in Fig. 8 in comparison with the "true" modal amplitudes obtained by projecting the DNS onto these modes, denoted $\hat{a}_{0,j}$.

Note that $\hat{a}^{(1)}_{0,1}$ and $\hat{a}^{(1)}_{0,2}$ are approximately confined to a "thickened" torus: each oscillating relatively quickly along a radius and drifting more slowly and chaotically around the circumference. The model fails to reproduce the radial motion, and caricatures the circumferential motion as a simple travelling wave with a relatively low period of 65.9 time units. It is clear from Fig. 8 that the average of the projected $(1,0,0)$, $(1,0,1)$ and $(1,0,2)$ modal amplitudes is well approximated by the travelling wave model: this is less true of the $(1,1,0)$ and $(1,1,\pm1)$ modal amplitudes, as indicated by Table 3, where the eigenvalues $\lambda^{(n)}_{n_x,n_z}$ are compared with the square of the travelling wave amplitudes $\|a^{(n)}_{n_x,n_z}\| = r^{(n)}_{n_x,n_z}$ (recall that the latter are twice the modal energies: §2.3).

The travelling wave solution is, however, entirely unsatisfactory from a dynamical viewpoint. The RMS modal velocities, calculated from

$$\mathrm{M}(n_x,n_z) = \frac{1}{\sqrt{L_x L_z}} \sum_n |a^{(n)}_{n_x,n_z}|, \tag{3.21}$$

are constant, since the modal amplitudes are constant: see the right panel of Fig. 9. The HKW regeneration cycle is completely absent. Here, and for similar plots in this paper, we present in the left panel the analogous quantities for the DNS with only those modes present in the low-dimensional model included in the projection, i.e. (3.21) with $a^{(n)}_{n_x,n_z}$

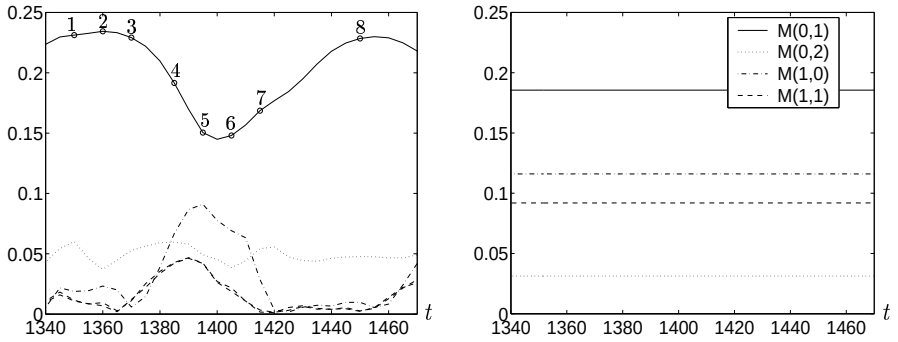

FIGURE 9. RMS modal velocities: from a representative cycle of the DNS (left, computed from (3.21) for $n = 1$, and thus slightly different from the right panel of Fig. 2) and analogous (constant) quantities for the coupled 6-mode model (right).

TABLE 4. Correlation coefficients for the 6-mode model.

n	n_x	n_z	$C(\widehat{T}^{(n)}_{n_x,n_z}, a^{(n)}_{n_x,n_z})$	$\beta^{(n)}_{n_x,n_z}$
1	0	1	-0.2650	0.0024
1	0	2	-0.8870	0.1294
1	1	0	-0.3086	0.0229
1	1	1	-0.5150	0.1039
1	1	-1	-0.5136	0.1038

replaced by $\hat{a}^{(n)}_{n_x,n_z}$. In neither case do we sum over n, since only one quantum number is included in the models considered in this paper.

Substituting (3.20) into the Galerkin approximation (2.4) yields

$$\mathbf{u}(\mathbf{x},t) = \sum \frac{r^{(n)}_{n_x,n_z}}{\sqrt{L_x L_z}} \exp\left(2\pi i \left(\frac{n_x x}{L_x} + \frac{n_z(z - \frac{\omega L_z t}{2\pi})}{L_z} + \frac{\alpha^{(n)}_{n_x,n_z}}{2\pi}\right)\right) \boldsymbol{\phi}^{(n)}_{n_x,n_z}(y), \quad (3.22)$$

hence the travelling waves (3.20) represent streak/vortex structures moving in the spanwise direction at speed $\omega L_z/(2\pi)$.

3.4.2. *The 6-mode model with losses to neglected modes*

We now attempt to improve the model behaviour by including energy transfer to neglected modes, using the ideas of §3.3. The resulting correlation coefficients and optimal damping values, calculated from (3.11-3.17), are presented in Table 4. There is significant variation in $C(\widehat{T}^{(n)}_{n_x,n_z}, a^{(n)}_{n_x,n_z})$, indicating that the quality of the linear damping approximation varies widely. To illustrate, we exhibit the best- and worst-approximated modes in Figs. 10 and 11, respectively. Averaging this variability via (3.18-3.19), we obtain the eddy viscosity $\nu = 0.0333$.

We now adjust the $\mathcal{O}(1)$ parameter α to obtain the best fit between the behaviour of the model and the DNS by computing a bifurcation diagram using the program AUTO (Doedel *et al.* (1997)), shown schematically in Fig. 12. This shows how existence and stability of solutions depends on α. As α increases from zero, we successively encounter the previously-described travelling waves (TW), modulated travelling waves (MW), and two different types of standing waves confined to a rotated version of the

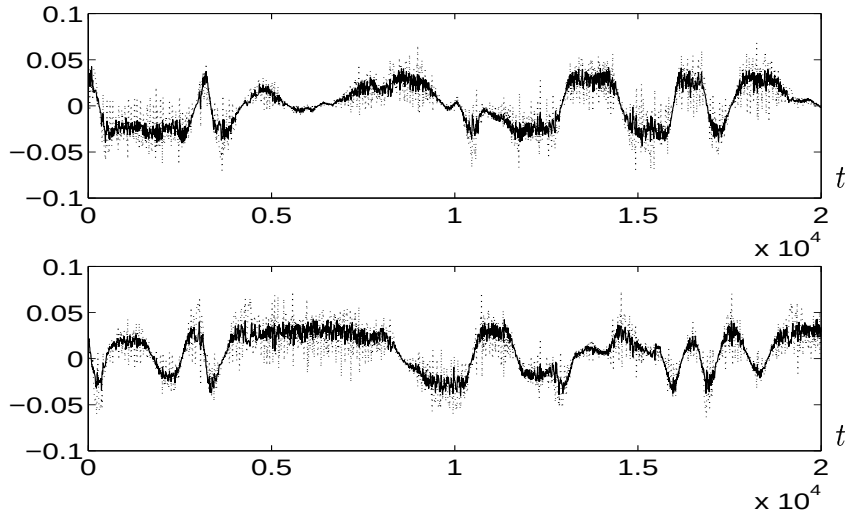

FIGURE 10. For the coupled 6-mode model: plot of $\Re(-\beta_{0,2}^{(1)}\hat{a}_{0,2}^{(1)})$ (solid) and $\Re(\widehat{T}_{0,2}^{(1)})$ (dashed) against time, t (top); plot of $\Im(-\beta_{0,2}^{(1)}\hat{a}_{0,2}^{(1)})$ (solid) and $\Im(\widehat{T}_{0,2}^{(1)})$ (dashed) against time, t (bottom). This reflects the high correlation coefficient of -0.8870 of Table 4.

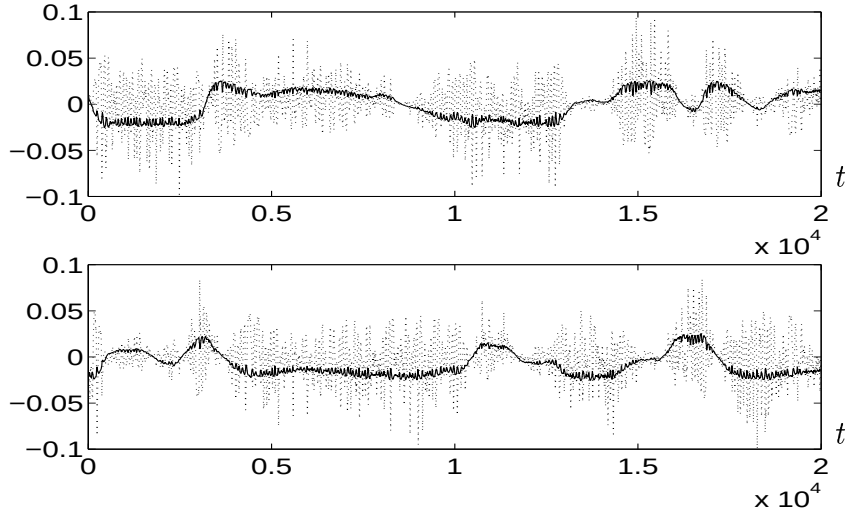

FIGURE 11. For the coupled 6-mode model: plot of $\Re(-10\beta_{0,1}^{(1)}\hat{a}_{0,1}^{(1)})$ (solid) and $\Re(\widehat{T}_{0,1}^{(1)})$ (dashed) against time, t (top); plot of $\Im(-10\beta_{0,1}^{(1)}\hat{a}_{0,1}^{(1)})$ (solid) and $\Im(\widehat{T}_{0,1}^{(1)})$ (dashed) against time, t (bottom). The optimal least-squares approximation in this case, with $\beta = -0.0024$ is essentially flat; we have multiplied this damping factor by 10 to show that the linear approximation (3.15) captures some of the low-frequency part of the noisy $\widehat{T}_{0,1}^{(1)}$ term. This reflects the low correlation coefficient of -0.2650 of Table 4.

real subspace: (SW_1 and SW_2). Schematic diagrams of the behaviour of the $(1,0,1)$ and $(1,0,2)$ modal amplitudes for these solutions are shown at the bottom of Fig. 12; at left are the travelling wave solutions shown in Fig. 8. All solutions with the exception of MW are stable over some interval of α. We draw the reader's attention to the branch of fixed points at right, which are produced in a pitchfork bifurcation from the laminar state at

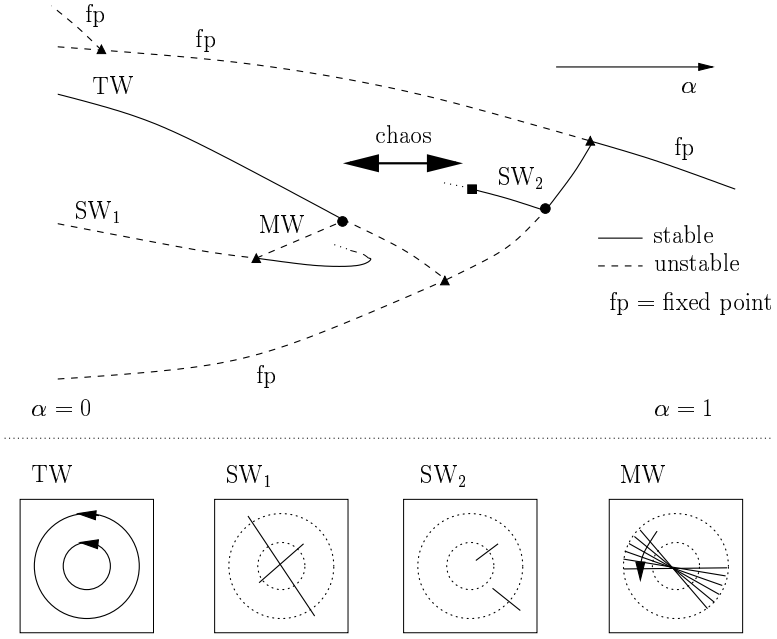

FIGURE 12. Schematic bifurcation diagram with respect to α for the modified coupled 6-mode model.

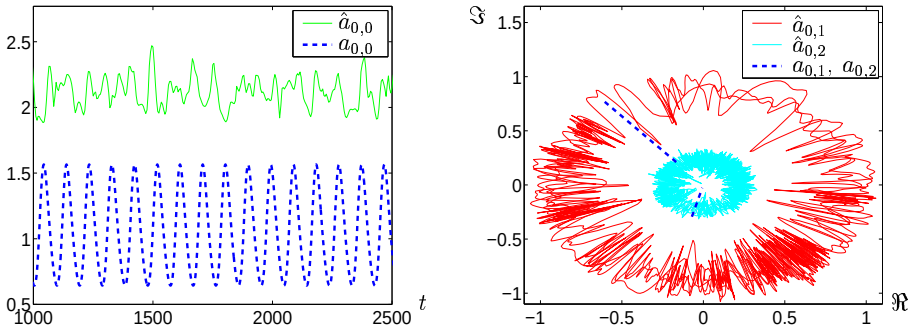

FIGURE 13. Behaviour of the modified coupled 6-mode model compared to the DNS projected onto the $(1,0,0)$ (left) and $(1,0,1)$, $(1,0,2)$ modes (right).

a higher value of α (~ 1.4); indeed, as we noted in §3.2 the laminar state of this model is unstable for Reynolds numbers in the vicinity of $Re = 400$.

The SW_2 solution, for which the $(1,0,1)$ and $(1,0,2)$ modal amplitudes oscillate along radii, captures the appropriate DNS dynamics. A representation analogous to Fig. 8 for $\alpha = 0.8$ appears as Fig. 13. However, while the amplitudes of the complex modes are reasonable, the amplitude of the $(1,0,0)$ mode in the model is significantly lower than in the projected DNS.

The RMS modal velocities for the model, calculated from (3.21), are presented in the right panel of Fig. 14, for comparison with analogous DNS quantities, re-plotted in the left panel (cf. Fig. 2). The cyclic behaviour is essentially reproduced: $\mathrm{M}(0,1)$ and $\mathrm{M}(1,0)$ are approximately of opposite phase, while the latter is approximately in phase with $\mathrm{M}(1,1)$. The magnitudes of the RMS modal velocities also compare well with those from the DNS.

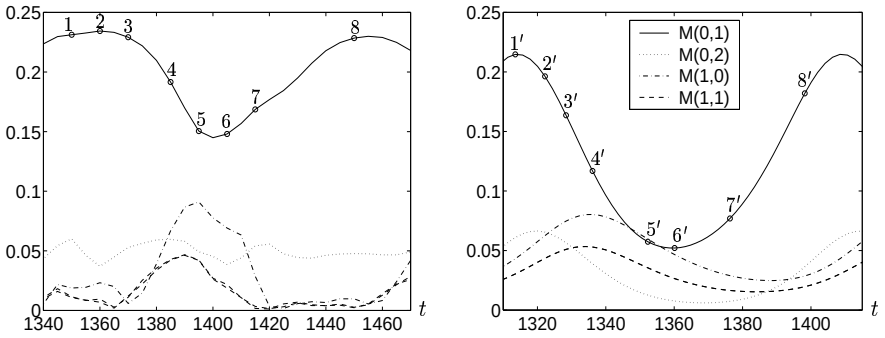

FIGURE 14. RMS modal velocities: from a representative cycle of the DNS (left, repeated from Fig. 9) and for one period from the coupled 6-mode model, including modelling of losses to neglected modes with $\alpha = 0.8$ (right).

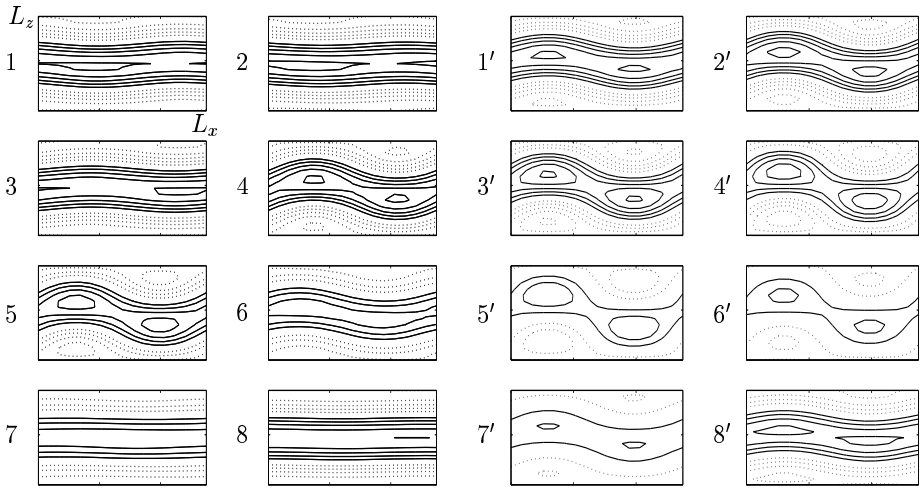

FIGURE 15. The streak breakdown process viewed in the (x, z) plane lying between the two plates in PCF: DNS projected onto the 6 modes present in the model (left) and computed from one period of the 6-mode coupled model (right).

In Figs. 15 and 16 we show reconstructed model velocity fields at the time instants 1'-8' marked on the right panel of Fig. 14 (analogous to 1-8 on the left), for comparison with analogous quantities from the DNS. The left panels of these figures repeat data from Figs. 3 and 4, but projected only onto the 6 modes present in the model (so the majority of the small scales is removed, leaving essential large scale structures). Fig. 15 shows that the solution provides reasonable reconstructions of the streak-breakdown process in the (x, z) mid-plane, although Fig. 16 indicates that the agreement between the streamwise velocity contours (as calculated from the streamwise-invariant modes) is somewhat less striking. This is largely due to the low amplitude of the $(1, 0, 0)$ mode: subtracting the laminar solution to obtain Fig. 17, we observe much more striking similarity between the DNS and the low-dimensional model.

Finally we compute turbulent statistics for the model by reconstructing the velocity field over one period of the limit cycle and calculating mean velocity fluctuations (u', v', w'). Fig. 18 compares these with analogous DNS quantities. We note good qual-

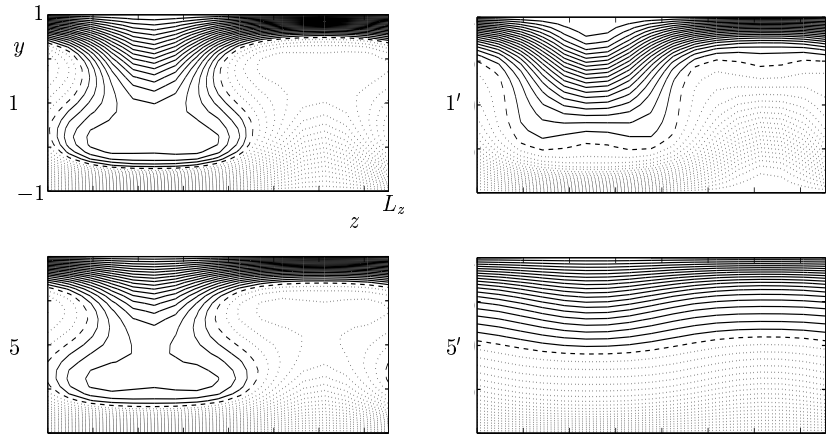

FIGURE 16. Streamwise velocities in the (y, z) plane calculated from the streamwise invariant modes and the laminar state: projection of the DNS onto the 6 modes present in the model (left) and computed from the 6-mode coupled model (right).

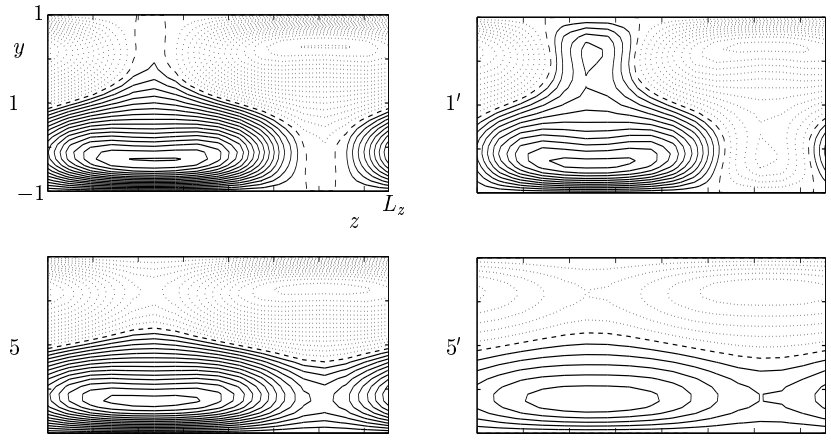

FIGURE 17. Streamwise velocities in the (y, z) plane calculated from the streamwise invariant modes only (excluding the laminar state): projection of the DNS onto the 6 modes present in the model (left) and computed from the 6-mode coupled model (right).

itative agreement for streamwise and spanwise RMS fluctuations ($\sqrt{\langle u'^2 \rangle}$ and $\sqrt{\langle v'^2 \rangle}$, respectively) and also for Reynolds stress ($\langle u'v' \rangle$). The qualitative agreement is less striking in the wall-normal direction ($\sqrt{\langle w'^2 \rangle}$), with a peak dominating the central portion between the two flat plates rather than a valley, although quantitative agreement is better.

3.4.3. *The 9-mode model*

Adding the $(1, 0, 3)$ mode to the 6-mode model considered above produces similar dynamic behaviour: in particular, the travelling waves (3.20) persist and the energy budget of the leading four model modes remains reasonable, as Table 5 indicates. Moreover, addition of damping to this model to represent losses to neglected modes produces a periodic orbit with behaviour similar to that of the damped 6-mode model of §3.3.

However, if we add the $(1, 1, \pm 2)$ modes to obtain the "full" set of equations (3.8) of the 9-mode model, the dynamic behaviour changes markedly: instead of travelling wave solutions we now observe chaos, as illustrated in Fig. 19. But while the amplitude coef-

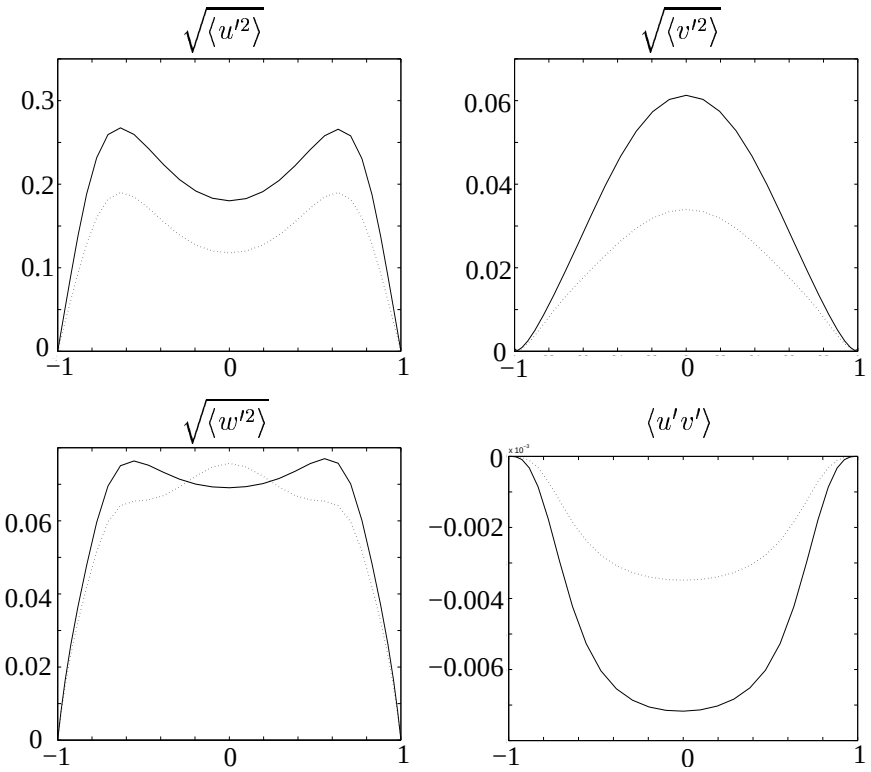

FIGURE 18. Performance of the 6-mode model measured by turbulent statistics with DNS (solid) and model (dotted) shown.

TABLE 5. Mean behaviour of the naive coupled "6-mode + $(1, 0, \pm 3)$" model.

(n, n_x, n_y)	$\lambda^{(n)}_{n_x,n_z}$	$(r^{(n)}_{n_x,n_z})^2$
$(1, 0, 0)$	4.4550	4.0487
$(1, 0, \pm 1)$	0.7821	0.7047
$(1, 0, \pm 2)$	0.0543	0.0318
$(1, \pm 1, 0)$	0.0386	0.2553
$(1, \pm 1, 1)$	0.0090	0.1140
$(1, \pm 1, -1)$	0.0090	0.2345
$(1, 0, \pm 3)$	0.0543	0.0006

ficients explore an appropriate region of phase space, the dynamics do not approximate the thickened tori of Fig. 8. Nor did it seem possible to improve the behaviour of this model by addition of eddy viscosity terms. Accordingly, we shall discuss this model no further here, although we shall see in §4 that an uncoupled version of it produces much more relevant behaviour.

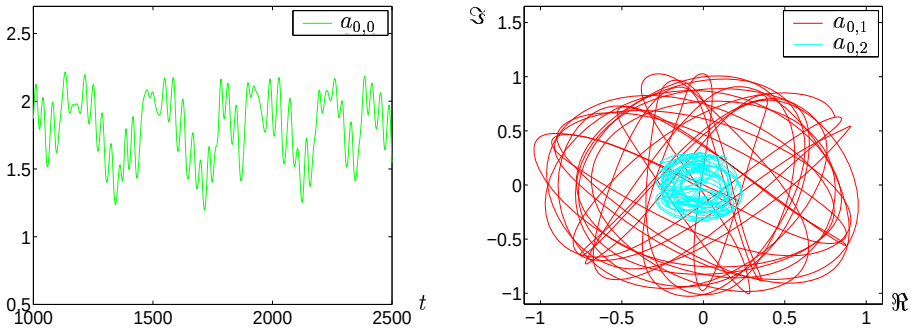

FIGURE 19. Behaviour of the coupled 9-mode model: evolution of $a_{0,0}^{(1)}$ versus time (left) and evolution of $a_{0,1}^{(1)}$ and $a_{0,2}^{(1)}$ in the complex plane (right).

4. Uncoupled low dimensional models

Commenting on the wall layer model of Aubry *et al.* (1988) with only streamwise-invariant modes ($n_x = 0$ in the present notation) presented in Holmes (1990), Moffatt (1990) pointed out that, if streamwise and cross-stream components are allowed to evolve independently, as they can in real flows, all disturbances eventually decay in the absence of streamwise variations. Indeed, for streamwise-invariant flow, where the convective derivative reduces to

$$D/Dt = \partial/\partial t + u_2\partial/\partial y + u_3\partial/\partial z, \tag{4.1}$$

the x-component of the Navier Stokes equation is

$$\frac{D}{Dt}(U + u_1) = \frac{1}{Re}\left(\frac{\partial^2}{\partial y^2} + \frac{\partial^2}{\partial z^2}\right)(U + u_1), \tag{4.2}$$

where U denotes the laminar profile, entirely in the x-direction, and $u_{1,2,3}$ are the fluctuations. Furthermore, it can be shown that

$$\frac{d}{dt}\int\int (u_2^2 + u_3^2)\, dydz = -2\nu\left\{\int\int \omega_x^2 dydz\right\}, \tag{4.3}$$

where ω_x is the x-component of the vorticity, showing that the energy in the cross-stream components of the velocity must decay to zero. In the long-time limit then, in (4.2), $D/Dt \to \partial/\partial t$, giving a simple diffusion equation for u_1. Thus for large time u_1 tends to a constant value, the only possible solution being $u_1 = 0$. Hence, although the streamwise velocity may experience transient growth due the cross-stream flow, it must also eventually vanish.

As pointed out in an addendum to Holmes (1990) and in more detail in Berkooz *et al.* (1991), the vector-valued POD eigenfunctions impose coupling between streamwise and cross-stream components in each mode. In particular, this implies that the inner product in the second term in the linear coefficients $\hat{A}_{n_x,n_z}^{(n,k)}$ of Eqn. (3.2) with $n_x = 0$ is nonzero, and, in fact, positive. This term provides the energy source. The constraint imposed by projection onto streamwise-invariant modes that (correctly) represent the typical behaviour with streamwise fluctuations present, imposes coupling that can maintain streamwise velocity fluctuations. To remove this constraint, we must allow the streamwise and cross-stream velocity components of streamwise invariant modes to evolve separately.

4.1. *Uncoupled basis functions*

Following the suggestion of Waleffe (1995*b*), we construct a pair of "uncoupled" basis functions from each empirical eigenfunction by decomposing it into mutually orthogonal components:

$$\mathbf{\Phi}^{(n)}_{n_x,n_z}(\mathbf{x}) = \mathbf{\Phi}^{(n)[1]}_{n_x,n_z}(\mathbf{x}) + \mathbf{\Phi}^{(n)[2]}_{n_x,n_z}(\mathbf{x}), \tag{4.4}$$

where

$$\mathbf{\Phi}^{(n)[1]}_{n_x,n_z}(\mathbf{x}) \stackrel{\text{def}}{=} P_{n_x,n_z}\mathbf{\Phi}^{(n)}_{n_x,n_z}(\mathbf{x}),\ \mathbf{\Phi}^{(n)[2]}_{n_x,n_z}(\mathbf{x}) \stackrel{\text{def}}{=} (I - P_{n_x,n_z})\mathbf{\Phi}^{(n)}_{n_x,n_z}(\mathbf{x}) \tag{4.5}$$

and the projection matrix is defined by

$$P_{n_x,n_z} \stackrel{\text{def}}{=} pp^T/(p^Tp) \text{ with } p \stackrel{\text{def}}{=} [-2\pi n_z/L_z, 0, 2\pi n_x/L_x]^T. \tag{4.6}$$

Here $\mathbf{\Phi}^{(n)[1]}_{n_x,n_z}(\mathbf{x})$ and $\mathbf{\Phi}^{(n)[2]}_{n_x,n_z}(\mathbf{x})$ are of the form (2.3) with

$$\boldsymbol{\phi}^{(n)[1]}_{n_x,n_z}(y) = \begin{pmatrix} a\boldsymbol{\phi}^{(n)}_{1,n_x,n_z}(y) - b\boldsymbol{\phi}^{(n)}_{3,n_x,n_z}(y) \\ 0 \\ -b\boldsymbol{\phi}^{(n)}_{1,n_x,n_z}(y) + c\boldsymbol{\phi}^{(n)}_{3,n_x,n_z}(y) \end{pmatrix}, \tag{4.7}$$

and

$$\boldsymbol{\phi}^{(n)[2]}_{n_x,n_z}(y) = \begin{pmatrix} (1-a)\boldsymbol{\phi}^{(n)}_{1,n_x,n_z}(y) + b\boldsymbol{\phi}^{(n)}_{3,n_x,n_z}(y) \\ \boldsymbol{\phi}^{(n)}_{2,n_x,n_z}(y) \\ b\boldsymbol{\phi}^{(n)}_{1,n_x,n_z}(y) + (1-c)\boldsymbol{\phi}^{(n)}_{3,n_x,n_z}(y) \end{pmatrix}, \tag{4.8}$$

respectively, appearing in the place of $\boldsymbol{\phi}^{(n)}_{n_x,n_z}(y)$, and where

$$a \stackrel{\text{def}}{=} \frac{n_z^2/L_z^2}{n_x^2/L_x^2 + n_z^2/L_z^2}, \qquad b \stackrel{\text{def}}{=} \frac{n_x n_z/(L_x L_z)}{n_x^2/L_x^2 + n_z^2/L_z^2}, \qquad c \stackrel{\text{def}}{=} \frac{n_x^2/L_x^2}{n_x^2/L_x^2 + n_z^2/L_z^2}. \tag{4.9}$$

The streamwise- and spanwise-invariant modes therefore take the forms

$$\boldsymbol{\phi}^{(n)[1]}_{0,n_z}(y) = \begin{pmatrix} \boldsymbol{\phi}^{(n)}_{1,0,n_z}(y) \\ 0 \\ 0 \end{pmatrix}, \quad \boldsymbol{\phi}^{(n)[2]}_{0,n_z}(y) = \begin{pmatrix} 0 \\ \boldsymbol{\phi}^{(n)}_{2,0,n_z}(y) \\ \boldsymbol{\phi}^{(n)}_{3,0,n_z}(y) \end{pmatrix}, \tag{4.10}$$

$$\boldsymbol{\phi}^{(n)[1]}_{n_x,0}(y) = \begin{pmatrix} 0 \\ 0 \\ \boldsymbol{\phi}^{(n)}_{3,n_x,0}(y) \end{pmatrix}, \quad \boldsymbol{\phi}^{(n)[2]}_{n_x,0}(y) = \begin{pmatrix} \boldsymbol{\phi}^{(n)}_{1,n_x,0}(y) \\ \boldsymbol{\phi}^{(n)}_{2,n_x,0}(y) \\ 0 \end{pmatrix}, \tag{4.11}$$

and for modes with neither streamwise nor spanwise variation we have $\boldsymbol{\phi}^{(n)[1]}_{0,0}(y) = 0$, $\boldsymbol{\phi}^{(n)[2]}_{0,0}(y) = \boldsymbol{\phi}^{(n)}_{0,0}(y)$. We also note that the functions are pairwise-orthogonal and divergence-free:

$$(\mathbf{\Phi}^{(n)[m]}_{n_x,n_z}(\mathbf{x}), \mathbf{\Phi}^{(n')[m']}_{n_x,n_z}(\mathbf{x})) = e^{(n)[m]}_{n_x,n_z}\delta_{nn'}\delta_{mm'}, \tag{4.12}$$

$$\nabla \cdot \mathbf{\Phi}^{(n)[m]}_{n_x,n_z}(\mathbf{x}) \quad = \quad 0 \text{ for } m = 1, 2. \tag{4.13}$$

We do not normalise the uncoupled modes, hence the (non-unity) coefficients $e^{(n)[m]}_{n_x,n_z}$; however, we have $e^{(n)[1]}_{n_x,n_z} + e^{(n)[2]}_{n_x,n_z} = 1$.

For $n_x = 0$ we recover the decomposition of Berkooz *et al.* (1991), but in general neither term in the decomposition represents a purely streamwise or cross-stream component. For

TABLE 6. Invariant subspaces for equations (5.1-5.16): variables omitted from each set $\{\ldots\}$ remain zero in the subspace concerned. Numbers in parentheses refer to restrictions to the real subspace.

invariant subspace	dimension
$\mathcal{S}_5 \equiv \{a_{00}^{(1)}, a_{02}^{(1)[1,2]}, a_{11}^{(1)[1,2]} = -a_{1-1}^{(1)[1,2]}\}$	9 (5)
$\mathcal{S}_6 \equiv \{a_{00}^{(1)}, a_{02}^{(1)[1,2]}, a_{10}^{(1)}, a_{12}^{(1)[1,2]} = a_{1-2}^{(1)[1,2]}\}$	11 (6)
$\mathcal{S}_8 \equiv \{a_{00}^{(1)}, a_{02}^{(1)[1,2]}, a_{10}^{(1)}, a_{11}^{(1)[1,2]} = a_{1-1}^{(1)[1,2]}, a_{12}^{(1)[1,2]} = a_{1-2}^{(1)[1,2]}\}$	15 (8)
$\mathcal{S}_{12} \equiv \{a_{00}^{(1)}, a_{01}^{(1)[1,2]}, a_{02}^{(1)[1,2]}, a_{03}^{(1)[1,2]}, a_{10}^{(1)}, a_{11}^{(1)[1,2]} = -a_{1-1}^{(1)[1,2]}, a_{12}^{(1)[1,2]} = a_{1-2}^{(1)[1,2]}\}$	23 (12)

$n_x, n_z \neq 0$, $\boldsymbol{\phi}_{n_x,n_z}^{[1]}(y)$ represents a structure that lies parallel with the walls at $y = \pm 1$, while $\boldsymbol{\phi}_{n_x,n_z}^{[2]}(y)$ is fully three-dimensional, cf. (4.7-4.8).

4.2. *Structure of the projected ODEs*

Uncoupling the $(1,0,1)$, $(1,0,2)$, $(1,0,3)$, $(1,1,\pm 1)$, and $(1,1,\pm 2)$ POD modes as outlined above and projecting Eqn. (1.1) onto these modes along with the single-component $(1,0,0)$ and $(1,1,0)$ POD modes, we obtain ODEs for the following set of modal amplitudes:

$$\mathbf{a}^{UC} = \left(a_{0,0}^{(1)}, a_{0,1}^{(1)[1,2]}, a_{0,2}^{(1)[1,2]}, a_{1,0}^{(1)}, a_{1,1}^{(1)[1,2]}, a_{1,-1}^{(1)[1,2]}, a_{0,3}^{(1)[1,2]}, a_{1,2}^{(1)[1,2]}, a_{1,-2}^{(1)[1,2]}\right),$$

These equations are too lengthy to display here, but have similar structure to the coupled equations, with important differences in the linear terms to be subsequently described. We list them in the Appendix as (5.1-5.16). We note that $a_{0,0}^{(1)}$ is real, all other modal amplitudes are complex, and that all modes other than $a_{0,0}^{(1)}$ and $a_{1,0}^{(1)}$ appear in pairs. Counting each complex mode as two real dimensions, this 9-mode uncoupled model is therefore 31-dimensional.

There are numerous invariant subspaces resulting from the $O(2) \times O(2)$ symmetries inherited by the ODEs, as detailed in Smith (2003). In what follows we need only one of these: the subspace

$$S_{12} \stackrel{\text{def}}{=} \{\mathbf{a}^{UC} \,|a_{1-1}^{(1)[1,2]} = -a_{11}^{(1)[1,2]} \;\text{ and }\; a_{1-2}^{(1)[1,2]} = a_{12}^{(1)[1,2]}\}, \tag{4.14}$$

but to illustrate how the full phase space may be parsed by such invariant subspaces, we list four of them in Table 6.

4.3. *Dynamical behaviour of the uncoupled models*

4.3.1. *The uncoupled 6-mode model*

The equations for this truncation may be obtained from (5.1-5.10) by setting $a_{0,3}^{(1)[1,2]} = a_{1,2}^{(1)[1,2]} = a_{1,-2}^{(1)[1,2]} = 0$. As noted in §4, for any initial condition, the solution of an uncoupled expansion with zero streamwise variation must eventually decay to zero (all streamwise-invariant flows necessarily relax to the laminar state). It was hypothesised in Berkooz *et al.* (1991) that, during this transient, the system would display "ghosts" of the behaviour demonstrated in the coupled expansion. In the uncoupled 6 mode model, we include the $(1,1,0)$ and $(1,1,\pm 1)$ streamwise modes, which do provide a (genuine) source of energy, so one might reasonably expect sustained dynamic behaviour. In Fig. 20

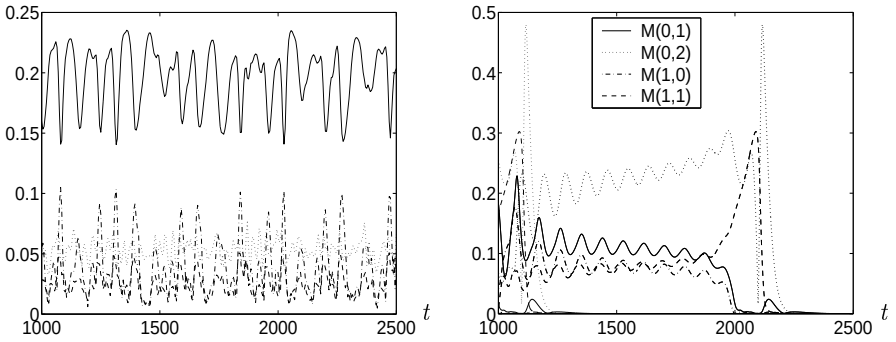

FIGURE 20. RMS modal velocities for the DNS (left) and computed from the uncoupled 6-mode model from (4.15). Note the differing scales on the ordinates of these two plots.

we plot the RMS modal velocities for this uncoupled model, computed via

$$\mathrm{M}(n_x, n_z) = \frac{1}{\sqrt{L_x L_z}} \sum_n \sqrt{e^{(n)[1]}_{n_x,n_z} |a^{(n)[1]}_{n_x,n_z}|^2 + e^{(n)[2]}_{n_x,n_z} |a^{(n)[2]}_{n_x,n_z}|^2}, \tag{4.15}$$

and observe that this is *not* the case. During the transient, however, the dynamics resemble the behaviour of §3.4 at $\alpha = 0.8$. In particular, the modal amplitudes are rapidly attracted to (some rotation of) the real subspace, and the transient oscillations have an approximate period of 87 non-dimensional time units.

4.3.2. *The uncoupled 9-mode model*

A primary motivation in considering uncoupled models is to remedy the problem of instability of the laminar state, exhibited by the coupled 6-mode model. Unfortunately, Eqns. (5.1-5.16) do not allow the laminar state to remain stable for all values of Re. Indeed, Eqn. (5.16) (as well as its close relation (5.14)) reveals that the trivial solution loses stability at

$$Re = -\frac{A'''_{12}}{A''''_{12}} = 577.6. \tag{4.16}$$

We may, of course, remedy this by adding eddy viscosity terms. Slightly generalizing the procedure of §3.3, we add a term of the form

$$-\alpha\nu(n_x^2 + n_z^2) a^{(n)[m]}_{n_x,n_z} \tag{4.17}$$

to each ODE, to find that the laminar state remains stable for all Re provided we choose α such that

$$\alpha > \frac{A''''_{12}}{5\,\nu\, e^{[2]}_{12}} = 0.2179, \tag{4.18}$$

(we retain $\nu = 0.0333$ as in the coupled 6-mode model). We therefore choose $\alpha = 0.22$ and compute bifurcation diagrams for steady and periodic states with respect to Re, with a view to comparisons with branches of steady solutions of the Navier Stokes equations.

4.3.3. *Dominant attractor at* $Re = 400$

The trivial solution is now stable, and solutions started sufficiently close to it approach it as $t \to \infty$. However, at $Re = 400$ almost all initial conditions of significant amplitude approach a periodic orbit lying within the S_{12} subspace. To explore the source of this attractor, we use AUTO (Doedel *et al.* (1997)) to follow its locus over a range of Reynolds

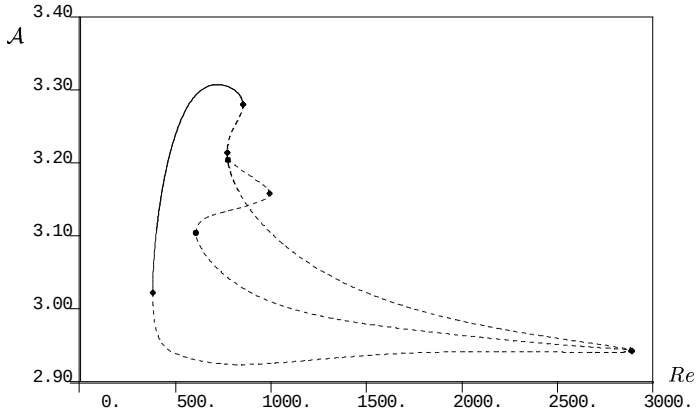

FIGURE 21. The isola of periodic orbits existing in the S_{12} subspace. Here and for the bifurcation diagram of Fig. 26, the ordinate $\mathcal{A}$ denotes the L^2 norm of the solution. Solid (resp., dashed) lines indicate stable (resp., unstable) solutions, and the dots indicate bifurcation points.

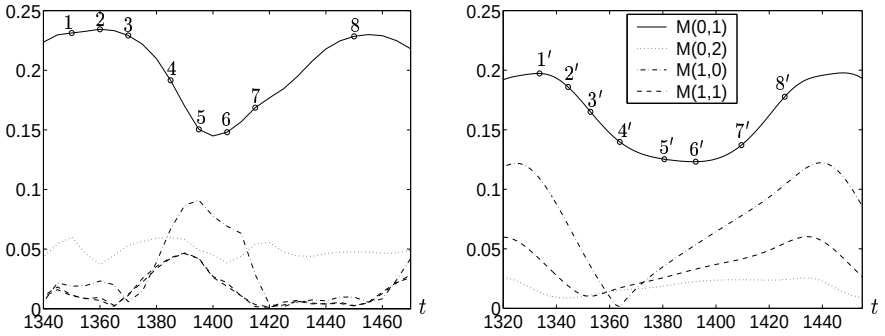

FIGURE 22. RMS modal velocities: from a representative cycle of the DNS (left, repeated from Fig. 9) and computed from one period of the uncoupled 9-mode model (right).

numbers, as shown in Fig. 21. We find that it arises in a saddle-node bifurcation at $Re \approx 379.8$ and loses stability in another saddle-node bifurcation at $Re \approx 852.8$, forming an isola. The remainder of the branch, and additional branches bifurcating from it, are all unstable. This is consistent with the observation that the MFU turbulent state appears as the Reynolds numbers passes between 300 and 400, cf., HKW.

RMS modal velocities for this model, calculated via (4.15), are compared with the same quantities for DNS in Fig. 22. Whilst magnitudes agree fairly well, phase relationships among the model's modal velocities are incorrect; in particular, $\mathrm{M}(0,1)$ and $\mathrm{M}(1,0)$ are now *in phase* and the model streak-breakdown process is consequently phase-shifted, as shown in Fig. 23. The velocity contours resulting from the streamwise-invariant modes in the model, shown in Fig. 24, are however much improved; here there is no need to subtract the laminar state to demonstrate qualitative agreement between model and DNS results.

In Fig. 25 we plot turbulence statistics for the uncoupled 9-mode model. In comparison to the analogous quantities for the coupled 6-mode model of Fig. 18, the RMS u' velocity is slightly improved, the RMS v' velocity is now larger than the DNS data rather than smaller, and while the RMS w' velocity is significantly greater (and worse) in magnitude, it now has the correct form, with a central valley rather than a peak. The Reynolds

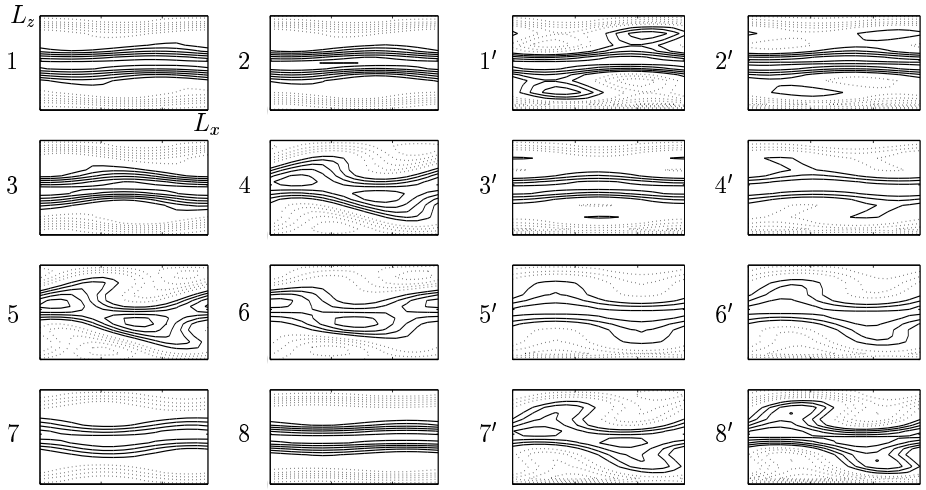

FIGURE 23. The streak breakdown process as viewed in the (x, z) plane lying between the two plates in PCF: DNS projected onto the 9 modes present in the model (left) and computed from one period of the uncoupled 9-mode model (right).

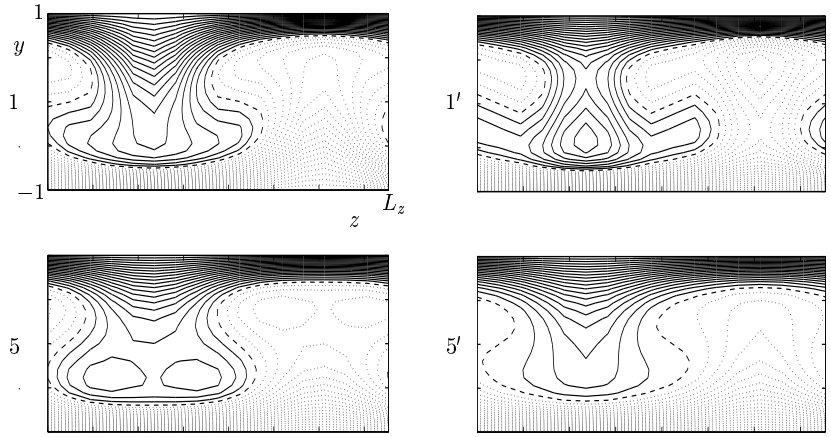

FIGURE 24. Streamwise velocities in the (y, z) plane calculated from the streamwise invariant modes and the laminar state: DNS projected onto the 9 modes present in the model (left) and computed from one period of the uncoupled 9-mode model (right).

stress, bottom right, is also improved, showing very good agreement between DNS and model in the near-wall region.

In addition to this periodic orbit, there are many other periodic and stationary states; some of the latter are shown in Fig. 26. With the exception of the stable laminar state represented by the solid line with amplitude $\mathcal{A} = 0$, these fixed points are generated in saddle-node bifurcations, predominantly in the range $Re = 200$–375, and they are all *unstable* with the exception of a single (modulo symmetry) stable state born in a saddle-node bifurcation at $Re \approx 220$, that becomes unstable in a supercritical Hopf bifurcation at $Re \approx 393$). These branches are qualitatively similar to those found by Schmiegel (1999) for the full Navier Stokes equations, cf. Nagata (1990); Clever & Busse (1992).

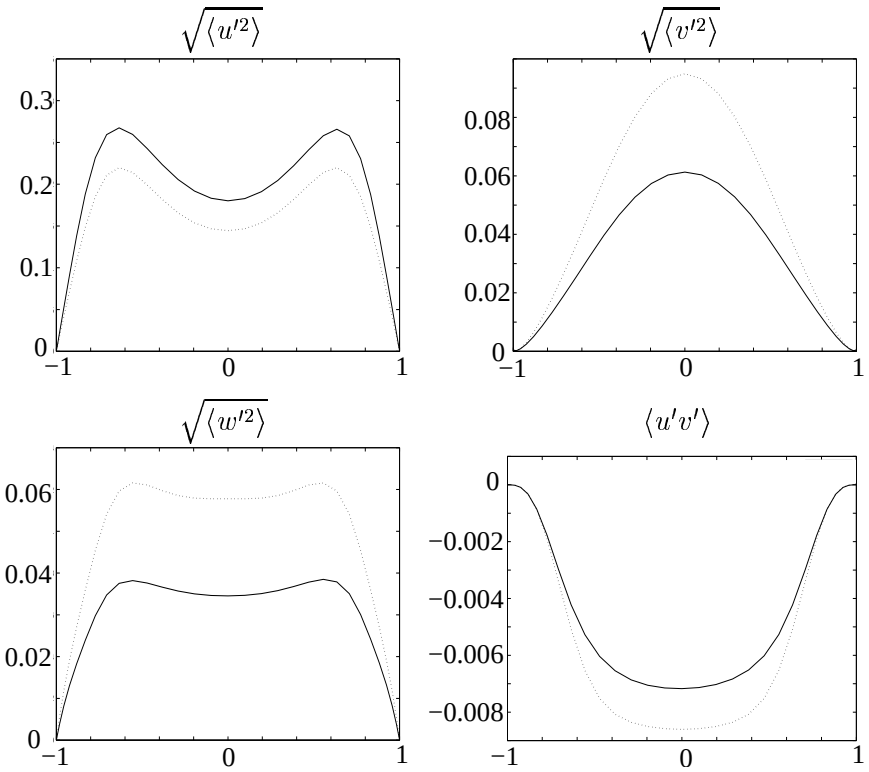

FIGURE 25. Performance of the 9-mode model measured by turbulent statistics with DNS (solid) and model (dotted) shown.

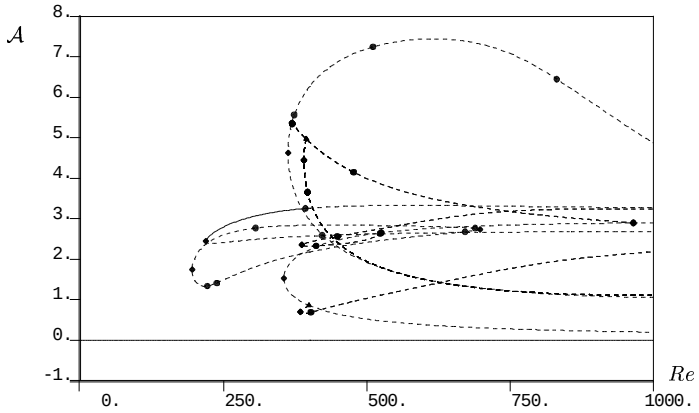

FIGURE 26. Branches of fixed points in the full phase space of the uncoupled 9-mode model. The stable laminar solution is represented by the solid line at $\mathcal{A} = 0$. Conventions are as in Fig. 21.

4.4. *Non-normality effects in the uncoupled models*

As noted in §1, the linear operator in Eqn. (1.1) is non-normal; however, the constraints among velocity components implicit in restriction to the first family of quantum numbers $n = 1$ in the coupled models of §3 render the linear part of Eqns. 3.8 diagonal (and hence very normal). The uncoupled expansion developed above restores non-normality, as may

be seen by examining Eqns. (5.1-5.16). In Smith (2003) eigenvalues and ϵ-pseudospectra of the linear part A^{UC} of these equations are examined using the theory of Trefethen (1992). As pointed out there, stable but highly non-normal operators with spectra lying close to the imaginary axis are likely to have ϵ-pseudospectra contours protruding into the right-hand half plane, and as demonstrated in Trefethen *et al.* (1993) this is the case for plane Couette flow at high Reynolds numbers, and for Poiseuille flow at Reynolds numbers slightly less than the critical value 5772. This in turn implies that certain linear modes can grow very large before eventually decaying, suggesting that small perturbations from the stable trivial solution might trigger a (nonlinear) transition to sustained turbulence.

We found that ϵ-pseudospectra contours for (5.1-5.16) do not penetrate far into the right-hand half plane, indicating that non-normality does not play a large role in the response of this system to perturbations. Nonetheless, we investigated the dynamical effects of non-normality via numerical simulations, samples of which for $\alpha = 0$ and $\alpha = 0.22$ are given in Figs. 27-28.

In the upper panel of each figure we follow the prescription in Baggett & Trefethen (1997) § III, setting

$$\mathbf{a}^{UC}(0) = C(\mathbf{a}^{UC}_{\max} + 0.1\ \mathbf{a}^{UC}_{\text{rand}}), \tag{4.19}$$

where $\mathbf{a}^{UC}_{\max}$ is a unit vector aligned with the most linearly unstable direction associated with A^{UC}, found through maximisation of $(d/dt)\|e^{tA^{UC}}\mathbf{a}^{UC}_{\max}\|$ at $t = 0$ subject to the constraint $\|\mathbf{a}^{UC}_{\max}\| = 1$. Obtaining this via the eigenvalue decomposition of $A^{UC} + (A^{UC})^T$ indicates that $\mathbf{a}^{UC}_{\max}$ may be chosen to align with the $a^{(1)[2]}_{1,\pm 2}$ directions. This is unsurprising in light of the discussion at the beginning of §4.3.2, where we noted that the $A'''_{1,2}$ linear term leads to linear instability of the laminar state, absent a model for losses to neglected modes. As noted in §3.2, the modes $a^{(1)}_{0,0}$ and $a^{(1)}_{1,\pm 2}$ span an invariant subspace in the coupled model; the span of $a^{(1)}_{0,0}$ and $a^{(1)[1,2]}_{1,\pm 2}$ is likewise invariant for the uncoupled model. Hence the random vector $\mathbf{a}^{UC}_{\text{rand}}$ in (4.19) is added to ensure that the system does not remain in this invariant subspace. In the lower panel of each figure we do not include $\mathbf{a}^{UC}_{\max}$ and choose our initial condition vector solely at random.

The results in Figs. 27-28 are representative of those found over many runs. In describing them we shall refer to "amplification factors", which we define to be the maximum of $\|\mathbf{a}^{UC}(t)\|/\|\mathbf{a}^{UC}(0)\|$. The initial amplification is certainly greater in the upper panel in each case (approximately 2.6 and 1.4 for $\alpha = 0$ and $\alpha = 0.22$ respectively) but all trajectories eventually decay, with the exception of the two cases $\alpha = 0$ and $\|\mathbf{a}^{UC}(0)\| = 1.0, 10^{0.5}$. In contrast, while the initial amplification is lower for the random initial data of the lower panel (1.4-2.1 for $\alpha = 0$ and 1.0 for $\alpha = 0.22$), more of these trajectories converge on the periodic orbit described in §4.3.2.

We thus conclude that, while non-normality may result in a modest amplification of suitably aligned initial conditions, this alone is generally insufficient to guarantee transition to the "turbulent" state. Indeed, the boundaries of the domains of attraction of both the trivial solution and the periodic orbit are likely to be complicated sets within the full phase space, and amplification in any one direction need not necessarily cause transition. Indeed, Eckhardt and colleagues (Schmiegel & Eckhardt (1997); Eckhardt & Mersmann (1999)) have shown that the full Navier Stokes equations (1.1) exhibit apparently fractal domain boundaries. With this in mind, it is unclear what linear analysis of the trivial state, normal or not, can reveal about transition.

The simulations with varying initial data uncover one other interesting feature of the uncoupled model. As Fig. 28 indicates, for $\alpha = 0.22$ most trajectories with initial conditions $\|\mathbf{a}^{UC}(0)\| = 10^{0.5}$ either decay "smoothly" to zero or converge on the periodic

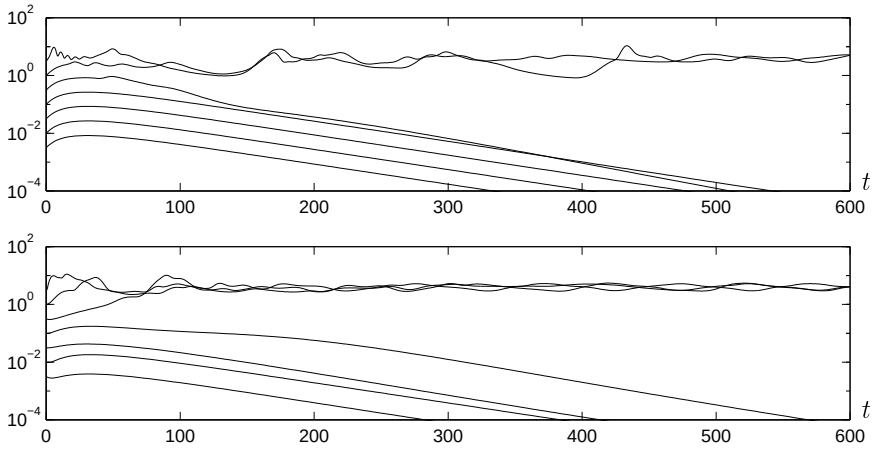

FIGURE 27. Transient behaviour of the 9-mode uncoupled model in the real subspace, with $\|\mathbf{a}^{UC}(t)\|$ plotted for solutions to (5.1-5.16) with $Re = 400$ and $\alpha = 0$. Initial amplitudes are given set to $\|\mathbf{a}^{UC}(0)\| = 10^{-2.5}$, 10^{-2}, $10^{-1.5}$, 10^{-1}, $10^{-0.5}$, 1, $10^{0.5}$. In the top panel the initial conditions are set according to (4.19), whereas in the bottom panel they are generated from purely random data.

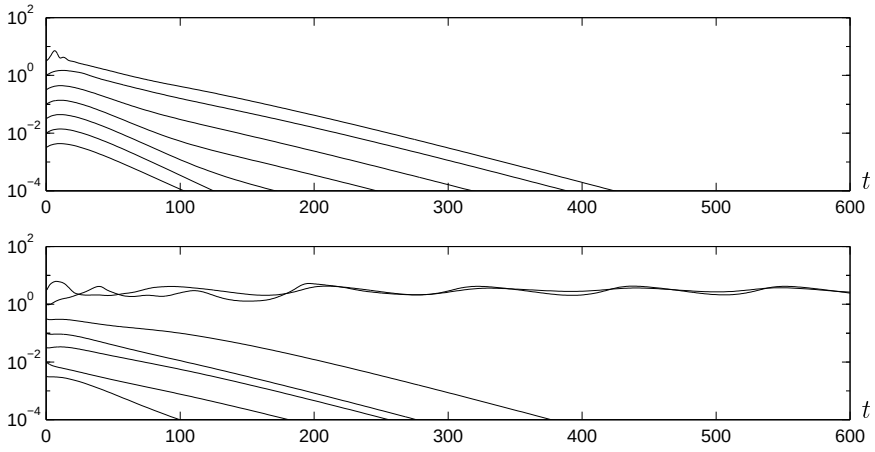

FIGURE 28. Transient behaviour of the 9-mode uncoupled model in the real subspace, with $\|\mathbf{a}^{UC}(t)\|$ plotted for solutions to (5.1-5.16) with $Re = 400$ and $\alpha = 0.22$. Initial amplitudes are given set to $\|\mathbf{a}^{UC}(0)\| = 10^{-2.5}$, 10^{-2}, $10^{-1.5}$, 10^{-1}, $10^{-0.5}$, 1, $10^{0.5}$. In the top panel the initial conditions are set according to (4.19), whereas in the bottom panel they are generated from purely random data.

orbit of Fig. 22, but a few initial conditions display long-lived transients, as illustrated in Fig. 29. Here the upper panel shows $\|\mathbf{a}^{UC}(t)\|$ on a normal Cartesian scale and in the lower panel we reconstruct the RMS modal velocities of (4.15). The behaviour is strikingly similar to that of the RMS modal velocities for the DNS (cf. Fig. 2) for several thousand time units, before collapsing the origin rather abruptly. This is reminiscent of the observed behaviour of numerical simulations of PCF in cases in which the spanwise dimension has been reduced to a value too small to sustain turbulence, e.g. as in HKW Fig. 20. We observed similar behaviour in our DNS simulations of the standard MFU domain for various initial conditions before arriving at the sustained behaviour of Fig.2.

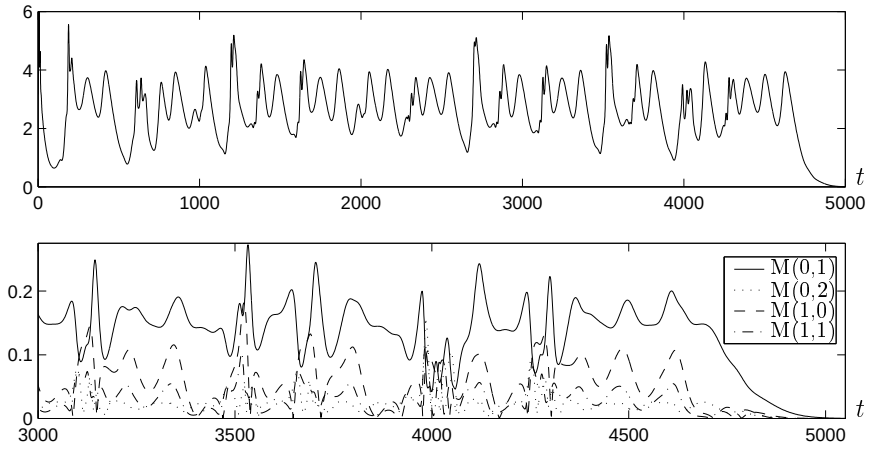

FIGURE 29. Transient behaviour of the 9-mode uncoupled model in the real subspace. $\|a(t)\|$ for solutions to (5.1-5.16) with $Re = 400$ and $\alpha = 0.22$. Initial amplitude is set to $\|\mathbf{a}^{UC}(0)\| = 10^{0.5}$. In the top panel $\|\mathbf{a}^{UC}(t)\|$ is plotted, while in the bottom panel we reconstruct the RMS modal velocities according to (4.15). This is to be compared with the behaviour in Fig. 22.

5. Conclusion

We open this concluding section with a brief survey of other low-dimensional models of shear-driven instability and turbulence, and then go on to summarise the principal contributions of this paper.

5.1. *Waleffe's models*

Waleffe proposed two models of turbulent PCF in the papers Waleffe (1995*a*,*b*, 1997) that followed HKW. Both are 4-dimensional quadratic ODEs of the form:

$$\frac{d}{dt}\begin{pmatrix} u \\ v \\ w \\ m \end{pmatrix} = \frac{1}{Re}\begin{pmatrix} \lambda_u u \\ \lambda_v v \\ \lambda_w w \\ \lambda_m m - \sigma_m \end{pmatrix} + \begin{pmatrix} 0 & 0 & -\sigma_w w & \sigma_u v \\ 0 & 0 & \sigma_v w & 0 \\ \sigma_w w & -\sigma_v w & 0 & -\sigma_m w \\ -\sigma_u v & 0 & \sigma_m w & 0 \end{pmatrix}\begin{pmatrix} u \\ v \\ w \\ m \end{pmatrix} \tag{5.1}$$

where the variables (u, v, w, m) respectively represent the amplitudes of spanwise modulation of the streamwise velocity, of the spanwise rolls, of an inflectional streak instability, and of the mean shear. Explicit expressions for the spatial fields of these modes are not given.

Waleffe (1995*b*) sets the parameters to $[\sigma_m, \sigma_u, \sigma_v, \sigma_w] = [0, 1, 1, 0.5]$ and $[\lambda_m, \lambda_u, \lambda_v, \lambda_w] = [-10, -10, -10, -15]$: this guarantees that the laminar state $(u, v, w, m) = (0, 0, 0, 1)$ is stable for all values of Re, and the bifurcation behaviour of (5.1) is then as follows. A saddle-node bifurcation of fixed points occurs at $Re = 98.6325$, creating stable and unstable steady solutions. The lower branch is unstable for all moderate values of Re; the initially stable upper branch becomes unstable in a supercritical Hopf bifurcation at $Re = 100.0232$ and the resulting periodic orbit remains stable until it disappears in a homoclinic bifurcation at $Re = 101.0311$. The laminar state is the only stable attractor in the range $101.0311 < Re < 356$, after which another stable periodic orbit appears in a second homoclinic bifurcation, remaining stable until it vanishes in a third homoclinic bifurcation at $Re \approx 435$: a time series for this periodic orbit at $Re = 400$ is shown in Fig. 30(a). Given the definitions of u and v above, one might infer that the RMS modal velocities associated with (5.1) can be expressed (in terms of (2.1)) as $v \sim$ M(0,1) and

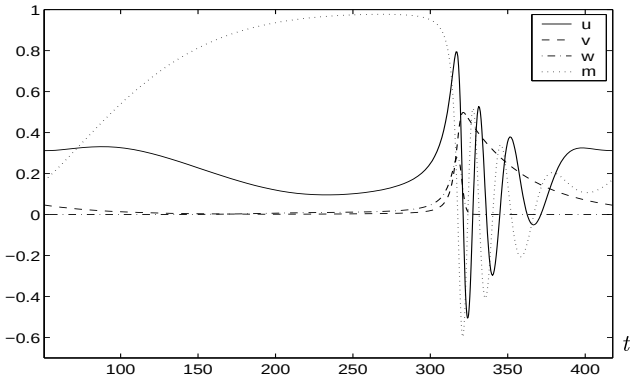

FIGURE 30. Behaviour of the periodic orbit of (5.1).

$u \sim$ M(1,0), in which case these would be *in* phase rather than antiphase, as in the MFU of HKW (cf. Fig. 2): alas, a periodic orbit alone does not a good model (for PCF in the MFU) make.

A similar model is considered in Waleffe (1997), which attempts to put (5.1) on firmer footing. Waleffe begins by considering sinusoidal shear flow – a channel subject to sinusoidal forcing with free-slip at the bounding walls – which is related, but not identical, to PCF. This (artificial) flow has the advantage that elementary trigonometric basis functions exist, yielding ODEs with analytically-determined coefficients. Waleffe projects the Navier Stokes equations onto eight (real) modes, and then imposes constraints among modal amplitudes to reduce first to a 5- and ultimately a 4-dimensional model. Although the rationale for these constraints seems unclear, the final result is a model "derived" from Navier Stokes, with parameters $[\sigma_m, \sigma_u, \sigma_v, \sigma_w] = [0.31, 1.29.0.22, 0.68]$ and $[\lambda_m, \lambda_u, \lambda_v, \lambda_w] = [2.47, 5.20, 7.67, 7.13]$. The most significant difference between this model and that in Waleffe (1995*a*,*b*) is the inclusion of a nonzero σ_m term, representing interaction between the mean shear and the streak instability. Waleffe (1997), p.894, then notes that "... an unstable limit cycle is generated ... for the parameter values of interest". This observation is supported by Dauchot and Vioujard's study of the system (Dauchot & Vioujard (2000)), in which Fig. 2 shows a saddle-node bifurcation which gives two unstable fixed points; one of these subsequently *gains* stability in a subcritical Hopf bifurcation in which an unstable periodic orbit branch appears. Dauchot and Vioujard discover regions of parameter space for which either no Hopf bifurcation occurs or a subcritical Hopf bifurcation occurs, yielding unstable periodic orbits. Nowhere is it claimed that the Hopf bifurcation is supercritical or stable periodic orbits exists, and parameter ranges in which the homoclinic bifurcation of Waleffe (1995*a*,*b*) might occur are not identified. Waleffe (1997) ends by quoting his previous stable periodic orbit, which does not exist for the parameters derived in Waleffe (1997), and (Waleffe 1997, Fig. 13) shows "some possible dynamics" for the four dimensional model. Thus, while (5.1) contains ingredients that can result in a regeneration cycle, parameter values for which this occurs do not seem derivable from fluid physics.

5.2. *Models of the Universität Marburg group*

Several low-dimensional models inspired by PCF have been considered by B. Eckhardt's group at the Universität Marburg, as detailed in Eckhardt & Mersmann (1999); Schmiegel & Eckhardt (1997); Schmiegel (1999). As in Waleffe (1997), these models were also constructed for sinusoidal shear flow. The most interesting among them have 9 and 19 de-

grees of freedom, and both exhibit transitional behaviour similar to PCF. In Eckhardt & Mersmann (1999) the evolution of perturbations for the 19-mode model is displayed in a plot similar to those of Figs. 27-28 above (although the critical perturbation amplitudes differ greatly). Similar information for the 9-mode model, which is essentially the 19-mode model restricted to an invariant subspace, is presented in three-dimensional form in Schmiegel (1999). In both instances, the fractal nature of the lifetime of perturbations is investigated; something which we did not address in this paper.

Various stationary states appear as Re is increased in the 19-mode model, the first in a saddle-node bifurcation at $Re \approx 190$. This is similar to full Navier Stokes results for PCF in Nagata (1990); Clever & Busse (1992) ($Re \approx 125$), and also to the present uncoupled 16-mode model of §4.3 ($Re \approx 195$: Fig. 26). In Schmiegel (1999) it is concluded that these stationary states have no dynamic significance, and instead it is collections of unstable periodic orbits which lead to the transition to turbulence by means of a "chaotic repeller." This contrasts with evidence that PCF turbulence arises through stationary states and heteroclinic orbits among them, also presented in Schmiegel (1999). We recall that in Moehlis *et al.* (2002) we also found, for the moderate aspect ratio domain, various complicated dynamics deriving from heteroclinic connections among stationary states. Schmiegel reasons that these low-dimensional models and the full PCF problem differ due to boundary conditions (free-slip for the sinusoidal shear flow of the models, no-slip for PCF). Eckhardt *et al.* (2004) also finds that collections of unstable periodic orbits are associated with a chaotic repellor and turbulence for a different 9-mode model for sinusoidal shear flow, which generalizes the 8-mode model of Waleffe (1997).

5.3. *Summary of the present results*

We believe that our attempts to model plane Couette flow in the Minimal Flow Unit have been a qualified success. We have examined two models in depth, one constructed from six and the other from nine POD modes. At Reynolds number 400, the 6-mode model has simple travelling waves with amplitudes that well-approximate the corresponding average DNS quantities. Since the POD is a dynamics-blind, statistical technique one might conclude that this is the best that can be done. However, adding damping terms to represent energy losses to neglected modes, the travelling waves were replaced periodic orbits confined to (a rotation of) the real subspace that showed good qualitative agreement with DNS statistics and quantitative agreement with DNS time-scales. Additionally, velocity field reconstructions analogous to those of HKW were also in agreement with DNS fields, at least for perturbations riding on the laminar solution.

We then performed the first analysis of *uncoupled* POD models, suggested by Berkooz *et al.* (1991) and independently by Waleffe (1995*b*). We found that the conjecture of Berkooz *et al.* (1991) that the uncoupled models would retain "ghosts" of the coupled model behaviour did not strictly hold true: the uncoupled 6-mode model gave unsustained behaviour; we could, however, relate this naive projection to the behaviour of the damped coupled 6-mode model. We then found that the 9-mode truncation, which did not lead to an interesting dynamic model with coupled modes, does yield a reasonable model when the modes are suitably uncoupled. We were able to remedy the problem of instability of the laminar state present in coupled models, and could also retain the cyclic regeneration behaviour found in this model. We also examined the influence of non-normality of the linear terms in the uncoupled model, finding that while it did weakly determine the initial response to perturbations, it is a poor indicator of whether the perturbations lead to "transition" to the non-trivial state, or collapse to laminar flow.

In both the 6-mode coupled and 9-mode uncoupled models, the attractor most relevant to the regeneration cycle is a standing wave periodic orbit. The projection of this onto

the three dominant modes ($(1,0,0),(1,0,1)$ and $(1,0,2)$) reveals that it involves a cyclic transfer of energy among the mean flow $\sim (1,0,0)$ (Fig. 5) and streamwise-invariant vortical structures with differing cross-stream scales $\sim (1,0,1),(1,0,2)$ (Fig. 6). However, although these three modes capture 93.5% of the energy on average, at least three further modes (albeit containing less than 1.3%) are required to sustain the dynamics; notably, these include the streamwise-varying $(1,1,0)$ and $(1,1,\pm 1)$ modes. The most striking qualitative deficiency of both models is their inability to reproduce the irregularity of the regeneration cycle, which appears in projections onto the $(1,0,1)$ and $(1,0,2)$ modes as a rapid radial oscillation precessing slowly in the azimuthal direction (cf. Figs. 8 and 13, righthand panels). However, in studies of the 0:1:2 model (3.10) we have found combinations of parameters A_{n_x,n_y} at which standing waves and modulated traveling waves coalesce in "branch-point" bifurcations, giving a potential for such behavior (Smith *et al.* (2004)). Hence these three dominant modes, suitably damped and excited by a model for the neglected modes, might capture the regeneration cycle both qualitatively and quantitatively.

The moral of this paper is that low-dimensional modelling is an imperfect science or, perhaps more properly, an art. While the POD necessarily yields sets of modes that contain the majority of the average turbulent kinetic energy, it is a rather poor indicator of which modes are *essential to the dynamics*. Despite this, through judicious selection of model truncations and appropriate modelling of losses to neglected modes, one may use this technique to construct convincing low-dimensional models, the components (amplitudes and coefficients) of which derive directly from the Navier Stokes equations.

Acknowledgments: This work was supported by DoE: DE-FG02-95ER25238 (T.S. and P.H.) and a National Science Foundation Mathematical Sciences Postdoctoral Research Fellowship to J.M. We thank Clancy Rowley for allowing the use, and modification, of his channel flow code.

Appendix: ODEs for the uncoupled model

$$\begin{aligned}
\dot{a}^{(1)[1]}_{0,0} &= A_{00} a^{(1)[1]}_{0,0}/Re \\
&+ 2B_{01}\ \Re(a^{(1)[1]}_{0,1} a^{(1)[2]*}_{0,1}) - 2B_{02}\ \Re(a^{(1)[1]}_{0,2} a^{(1)[2]*}_{0,2}) - 2B_{03}\ \Re(a^{(1)[1]}_{0,3} a^{(1)[2]*}_{0,3}) \\
&+ 2B^{[1]}_{11}\ \Re(a^{(1)[1]}_{1,1} a^{(1)[2]*}_{1,1} + a^{(1)[1]}_{1,-1} a^{(1)[2]*}_{1,-1}) - B^{[2]}_{11}\ (|a^{(1)[2]}_{1,1}|^2 + |a^{(1)[2]}_{1,-1}|^2) \\
&+ 2B^{[1]}_{12}\ \Re(a^{(1)[1]}_{1,2} a^{(1)[2]*}_{1,2} + a^{(1)[1]}_{1,-2} a^{(1)[2]*}_{1,-2}) + B^{[2]}_{12}\ (|a^{(1)[2]}_{1,2}|^2 + |a^{(1)[2]}_{1,-2}|^2) \qquad (5.1)
\end{aligned}$$

$$
\begin{aligned}
e_{01}^{[1]}\ \dot{a}_{0,1}^{(1)[1]} &= A_{01}^{'} a_{0,1}^{(1)[1]}/Re + A_{01}^{''} a_{0,1}^{(1)[2]} - B_{01}\ a_{0,0}^{(1)[1]} a_{0,1}^{(1)[2]} \\
&+ {}^{0,1[1]}C_{1,-1[1]}^{1,0[1]} (a_{1,0}^{(1)[1]} a_{1,-1}^{(1)[1]*} - a_{1,1}^{(1)[1]} a_{1,0}^{(1)[1]*}) - {}^{0,1[1]}C_{0,1[2]}^{0,2[1]} a_{0,2}^{(1)[1]} a_{0,1}^{(1)[2]*} \\
&+ {}^{0,1[1]}C_{1,-1[2]}^{1,0[1]} (a_{1,0}^{(1)[1]} a_{1,-1}^{(1)[2]*} - a_{1,1}^{(1)[2]} a_{1,0}^{(1)[1]*}) \\
&- {}^{0,1[1]}C_{1,-2[1]}^{1,-1[1]} (a_{1,-1}^{(1)[1]} a_{1,-2}^{(1)[1]*} - a_{1,2}^{(1)[1]} a_{1,1}^{(1)[1]*}) - {}^{0,1[1]}C_{0,2[2]}^{0,3[1]} a_{0,3}^{(1)[1]} a_{0,2}^{(1)[2]*} \\
&+ {}^{0,1[1]}C_{1,-2[2]}^{1,-1[1]} (a_{1,-1}^{(1)[1]} a_{1,-2}^{(1)[2]*} - a_{1,2}^{(1)[2]} a_{1,1}^{(1)[1]*}) \\
&- {}^{0,1[1]}C_{1,-2[1]}^{1,-1[2]} (a_{1,-1}^{(1)[2]} a_{1,-2}^{(1)[1]*} - a_{1,2}^{(1)[1]} a_{1,1}^{(1)[2]*}) - {}^{0,1[1]}C_{0,2[1]}^{0,3[2]} a_{0,3}^{(1)[2]} a_{0,2}^{(1)[1]*} \\
&+ {}^{0,1[1]}C_{1,-2[2]}^{1,-1[2]} (a_{1,-1}^{(1)[2]} a_{1,-2}^{(1)[2]*} - a_{1,2}^{(1)[2]} a_{1,1}^{(1)[2]*})
\end{aligned} \tag{5.2}
$$

$$
\begin{aligned}
e_{01}^{[2]}\ \dot{a}_{0,1}^{(1)[2]} &= A_{01}^{'''} a_{0,1}^{(1)[2]}/Re - {}^{0,1[2]}C_{0,1[2]}^{0,2[2]} a_{0,2}^{(1)[2]} a_{0,1}^{(1)[2]*} + {}^{0,1[2]}C_{0,2[2]}^{0,3[2]} a_{0,3}^{(1)[2]} a_{0,2}^{(1)[2]*} \\
&- {}^{0,1[2]}C_{1,-1[1]}^{1,0[1]} (a_{1,0}^{(1)[1]} a_{1,-1}^{(1)[1]*} - a_{1,1}^{(1)[1]} a_{1,0}^{(1)[1]*}) \\
&- {}^{0,1[2]}C_{1,-1[2]}^{1,0[1]} (a_{1,0}^{(1)[1]} a_{1,-1}^{(1)[2]*} - a_{1,1}^{(1)[2]} a_{1,0}^{(1)[1]*}) \\
&+ {}^{0,1[2]}C_{1,-2[1]}^{1,-1[1]} (a_{1,-1}^{(1)[1]} a_{1,-2}^{(1)[1]*} - a_{1,2}^{(1)[1]} a_{1,1}^{(1)[1]*}) \\
&- {}^{0,1[2]}C_{1,-2[2]}^{1,-1[1]} (a_{1,-1}^{(1)[1]} a_{1,-2}^{(1)[2]*} - a_{1,2}^{(1)[2]} a_{1,1}^{(1)[1]*}) \\
&- {}^{0,1[2]}C_{1,-2[1]}^{1,-1[2]} (a_{1,-1}^{(1)[2]} a_{1,-2}^{(1)[1]*} - a_{1,2}^{(1)[1]} a_{1,1}^{(1)[2]*}) \\
&+ {}^{0,1[2]}C_{1,-2[2]}^{1,-1[2]} (a_{1,-1}^{(1)[2]} a_{1,-2}^{(1)[2]*} - a_{1,2}^{(1)[2]} a_{1,1}^{(1)[2]*})
\end{aligned} \tag{5.3}
$$

$$
\begin{aligned}
e_{02}^{[1]}\ \dot{a}_{0,2}^{(1)[1]} &= A_{02}^{'} a_{0,2}^{(1)[1]}/Re + A_{02}^{''} a_{0,2}^{(1)[2]} + B_{02} a_{0,0}^{(1)[1]} a_{0,2}^{(1)[2]} + {}^{0,1[1]}C_{0,1[2]}^{0,2[1]} a_{0,1}^{(1)[1]} a_{0,1}^{(1)[2]} \\
&- {}^{0,2[1]}C_{1,-2[1]}^{1,0[1]} (a_{1,0}^{(1)[1]} a_{1,-2}^{(1)[1]*} + a_{1,2}^{(1)[1]} a_{1,0}^{(1)[1]*}) + {}^{0,1[1]}C_{0,2[1]}^{0,3[2]} a_{0,3}^{(1)[2]} a_{0,1}^{(1)[1]*} \\
&- {}^{0,2[1]}C_{1,-2[2]}^{1,0[1]} (a_{1,0}^{(1)[1]} a_{1,-2}^{(1)[2]*} + a_{1,2}^{(1)[2]} a_{1,0}^{(1)[1]*}) - {}^{0,2[1]}C_{1,-1[2]}^{1,1[2]} a_{1,1}^{(1)[2]} a_{1,-1}^{(1)[2]*} \\
&- {}^{0,2[1]}C_{1,-1[2]}^{1,1[1]} (a_{1,1}^{(1)[1]} a_{1,-1}^{(1)[2]*} + a_{1,1}^{(1)[2]} a_{1,-1}^{(1)[1]*}) - {}^{0,2[1]}C_{0,1[2]}^{0,3[1]} a_{0,3}^{(1)[1]} a_{0,1}^{(1)[2]*}
\end{aligned} \tag{5.4}
$$

$$
\begin{aligned}
e_{02}^{[2]}\ \dot{a}_{0,2}^{(1)[2]} &= A_{02}^{'''} a_{0,2}^{(1)[2]}/Re + {}^{0,1[2]}C_{0,1[2]}^{0,2[2]} (a_{0,1}^{(1)[2]})^2 + {}^{0,2[2]}C_{1,-1[1]}^{1,1[1]} a_{1,1}^{(1)[1]} a_{1,-1}^{(1)[1]*} \\
&- {}^{0,2[2]}C_{1,-2[1]}^{1,0[1]} (a_{1,0}^{(1)[1]} a_{1,-2}^{(1)[1]*} + a_{1,2}^{(1)[1]} a_{1,0}^{(1)[1]*}) - {}^{0,2[2]}C_{1,-1[2]}^{1,1[2]} a_{1,1}^{(1)[2]} a_{1,-1}^{(1)[2]*} \\
&+ {}^{0,2[2]}C_{1,-2[2]}^{1,0[1]} (a_{1,0}^{(1)[1]} a_{1,-2}^{(1)[2]*} + a_{1,2}^{(1)[2]} a_{1,0}^{(1)[1]*}) - {}^{0,2[1]}C_{0,1[2]}^{0,3[2]} a_{0,3}^{(1)[2]} a_{0,1}^{(1)[2]*} \\
&- {}^{0,2[2]}C_{1,-1[2]}^{1,1[1]} (a_{1,1}^{(1)[1]} a_{1,-1}^{(1)[2]*} + a_{1,1}^{(1)[2]} a_{1,-1}^{(1)[1]*})
\end{aligned} \tag{5.5}
$$

$$\begin{aligned}
\dot{a}^{(1)[1]}_{1,0} &= A_{10}a^{(1)[1]}_{1,0}/Re + {}^{0,1[1]}C^{1,0[1]}_{1,-1[2]}(a^{(1)[1]}_{0,1}a^{(1)[2]}_{1,-1} - a^{(1)[2]}_{1,1}a^{(1)[1]*}_{0,1}) \\
&- {}^{0,2[1]}C^{1,0[1]}_{1,-2[2]}(a^{(1)[1]}_{0,2}a^{(1)[2]}_{1,-2} + a^{(1)[2]}_{1,2}a^{(1)[1]*}_{0,2}) \\
&- {}^{1,0[1]}C^{0,1[1]}_{1,-1[1]}(a^{(1)[1]}_{0,1}a^{(1)[1]}_{1,-1} - a^{(1)[1]}_{1,1}a^{(1)[1]*}_{0,1}) \\
&- {}^{1,0[1]}C^{0,1[2]}_{1,-1[1]}(a^{(1)[2]}_{0,1}a^{(1)[1]}_{1,-1} - a^{(1)[1]}_{1,1}a^{(1)[2]*}_{0,1}) \\
&+ {}^{1,0[1]}C^{0,1[2]}_{1,-1[2]}(a^{(1)[2]}_{0,1}a^{(1)[2]}_{1,-1} - a^{(1)[2]}_{1,1}a^{(1)[2]*}_{0,1}) \\
&+ {}^{1,0[1]}C^{0,2[1]}_{1,-2[1]}(a^{(1)[1]}_{0,2}a^{(1)[1]}_{1,-2} + a^{(1)[1]}_{1,2}a^{(1)[1]*}_{0,2}) \\
&- {}^{1,0[1]}C^{0,2[2]}_{1,-2[1]}(a^{(1)[2]}_{0,2}a^{(1)[1]}_{1,-2} + a^{(1)[1]}_{1,2}a^{(1)[2]*}_{0,2}) \\
&+ {}^{1,0[1]}C^{0,2[2]}_{1,-2[2]}(a^{(1)[2]}_{0,2}a^{(1)[2]}_{1,-2} + a^{(1)[2]}_{1,2}a^{(1)[2]*}_{0,2}) \qquad (5.6)
\end{aligned}$$

$$\begin{aligned}
e^{[1]}_{11}\ \dot{a}^{(1)[1]}_{1,1} &= A'_{11}a^{(1)[1]}_{1,1}/Re + A''_{11}a^{(1)[2]}_{1,1} - B^{[1]}_{11}a^{(1)[1]}_{0,0}a^{(1)[2]}_{1,1} + {}^{1,1[1]}C^{0,1[1]}_{1,0[1]}a^{(1)[1]}_{0,1}a^{(1)[1]}_{1,0} \\
&- {}^{1,1[1]}C^{0,1[2]}_{1,0[1]}a^{(1)[2]}_{0,1}a^{(1)[1]}_{1,0} + {}^{1,1[1]}C^{0,2[1]}_{1,-1[2]}a^{(1)[1]}_{0,2}a^{(1)[2]}_{1,-1} - {}^{1,1[1]}C^{0,2[2]}_{1,-1[1]}a^{(1)[2]}_{0,2}a^{(1)[1]}_{1,-1} \\
&+ {}^{1,1[1]}C^{0,2[2]}_{1,-1[2]}a^{(1)[2]}_{0,2}a^{(1)[2]}_{1,-1} + {}^{1,1[1]}C^{0,3[1]}_{1,-2[1]}a^{(1)[1]}_{0,3}a^{(1)[1]}_{1,-2} + {}^{1,1[1]}C^{0,3[1]}_{1,-2[2]}a^{(1)[1]}_{0,3}a^{(1)[2]}_{1,-2} \\
&- {}^{1,1[1]}C^{0,3[2]}_{1,-2[1]}a^{(1)[2]}_{0,3}a^{(1)[1]}_{1,-2} + {}^{1,1[1]}C^{0,3[2]}_{1,-2[2]}a^{(1)[2]}_{0,3}a^{(1)[2]}_{1,-2} - {}^{1,1[1]}C^{1,2[1]}_{0,1[1]}a^{(1)[1]}_{1,2}a^{(1)[1]*}_{0,1} \\
&- {}^{1,1[1]}C^{1,2[1]}_{0,1[2]}a^{(1)[1]}_{1,2}a^{(1)[2]*}_{0,1} - {}^{1,1[1]}C^{1,2[2]}_{0,1[1]}a^{(1)[2]}_{1,2}a^{(1)[1]*}_{0,1} \\
&+ {}^{1,1[1]}C^{1,2[2]}_{0,1[2]}a^{(1)[2]}_{1,2}a^{(1)[2]*}_{0,1} \qquad (5.7)
\end{aligned}$$

$$\begin{aligned}
e^{[2]}_{11}\ \dot{a}^{(1)[2]}_{1,1} &= A'''_{11}a^{(1)[2]}_{1,1}/Re + A''''_{11}a^{(1)[2]}_{1,1} + 0.5B^{[2]}_{11}a^{(1)[1]}_{0,0}a^{(1)[2]}_{1,1} + {}^{1,1[2]}C^{0,1[1]}_{1,0[1]}a^{(1)[1]}_{0,1}a^{(1)[1]}_{1,0} \\
&+ {}^{1,1[2]}C^{0,1[2]}_{1,0[1]}a^{(1)[2]}_{0,1}a^{(1)[1]}_{1,0} + {}^{1,1[2]}C^{0,2[1]}_{1,-1[1]}a^{(1)[1]}_{0,2}a^{(1)[1]}_{1,-1} + {}^{1,1[2]}C^{0,2[1]}_{1,-1[2]}a^{(1)[1]}_{0,2}a^{(1)[2]}_{1,-1} \\
&+ {}^{1,1[2]}C^{0,2[2]}_{1,-1[1]}a^{(1)[2]}_{0,2}a^{(1)[1]}_{1,-1} + {}^{1,1[2]}C^{0,2[2]}_{1,-1[2]}a^{(1)[2]}_{0,2}a^{(1)[2]}_{1,-1} + {}^{1,1[2]}C^{0,3[1]}_{1,-2[1]}a^{(1)[1]}_{0,3}a^{(1)[1]}_{1,-2} \\
&+ {}^{1,1[2]}C^{0,3[1]}_{1,-2[2]}a^{(1)[1]}_{0,3}a^{(1)[2]}_{1,-2} - {}^{1,1[2]}C^{0,3[2]}_{1,-2[1]}a^{(1)[2]}_{0,3}a^{(1)[1]}_{1,-2} + {}^{1,1[2]}C^{0,3[2]}_{1,-2[2]}a^{(1)[2]}_{0,3}a^{(1)[2]}_{1,-2} \\
&+ {}^{1,1[2]}C^{1,2[1]}_{0,1[1]}a^{(1)[1]}_{1,2}a^{(1)[1]*}_{0,1} - {}^{1,1[2]}C^{1,2[1]}_{0,1[2]}a^{(1)[1]}_{1,2}a^{(1)[2]*}_{0,1} - {}^{1,1[2]}C^{1,2[2]}_{0,1[1]}a^{(1)[2]}_{1,2}a^{(1)[1]*}_{0,1} \\
&+ {}^{1,1[2]}C^{0,1[2]}_{1,-2[2]}a^{(1)[2]}_{1,2}a^{(1)[2]*}_{0,1} \qquad (5.8)
\end{aligned}$$

$$\begin{aligned}
e^{[1]}_{11}\ \dot{a}^{(1)[1]}_{1,-1} &= A'_{11}a^{(1)[1]}_{1,-1}/Re + A''_{11}a^{(1)[2]}_{1,-1} - B^{[1]}_{11}a^{(1)[1]}_{0,0}a^{(1)[2]}_{1,-1} + {}^{1,1[1]}C^{1,2[1]}_{0,1[1]}a^{(1)[1]}_{0,1}a^{(1)[1]}_{1,-2} \\
&+ {}^{1,1[1]}C^{1,2[2]}_{0,1[1]}a^{(1)[1]}_{0,1}a^{(1)[2]}_{1,-2} + {}^{1,1[1]}C^{1,2[1]}_{0,1[2]}a^{(1)[2]}_{0,1}a^{(1)[1]}_{1,-2} - {}^{1,1[1]}C^{1,2[2]}_{0,1[2]}a^{(1)[2]}_{0,1}a^{(1)[2]}_{1,-2} \\
&- {}^{1,1[1]}C^{0,1[1]}_{1,0[1]}a^{(1)[1]}_{1,0}a^{(1)[1]*}_{0,1} + {}^{1,1[1]}C^{0,1[2]}_{1,0[1]}a^{(1)[1]}_{1,0}a^{(1)[2]*}_{0,1} \\
&- {}^{1,1[1]}C^{0,2[2]}_{1,-1[1]}a^{(1)[1]}_{1,1}a^{(1)[2]*}_{0,2} + {}^{1,1[1]}C^{0,2[1]}_{1,-1[2]}a^{(1)[2]}_{1,1}a^{(1)[1]*}_{0,2} \\
&+ {}^{1,1[1]}C^{0,2[2]}_{1,-1[2]}a^{(1)[2]}_{1,1}a^{(1)[2]*}_{0,2} - {}^{1,1[1]}C^{0,3[1]}_{1,-2[1]}a^{(1)[1]}_{1,2}a^{(1)[1]*}_{0,3} \\
&+ {}^{1,1[1]}C^{0,3[2]}_{1,-2[1]}a^{(1)[1]}_{1,2}a^{(1)[2]*}_{0,3} - {}^{1,1[1]}C^{0,3[1]}_{1,-2[2]}a^{(1)[2]}_{1,2}a^{(1)[1]*}_{0,3} \\
&- {}^{1,1[1]}C^{0,3[2]}_{1,-2[2]}a^{(1)[2]}_{1,2}a^{(1)[2]*}_{0,3} \qquad (5.9)
\end{aligned}$$

$$
\begin{aligned}
e_{11}^{[2]}\ \dot{a}_{1,-1}^{(1)[2]} &= A_{11}^{'''} a_{1,-1}^{(1)[2]}/Re + A_{11}^{''''} a_{1,-1}^{(1)[2]} + 0.5 B_{11}^{[2]} a_{0,0}^{(1)[1]} a_{1,-1}^{(1)[2]} - {}^{1,1[2]}C_{0,1[1]}^{1,2[1]} a_{0,1}^{(1)[1]} a_{1,-2}^{(1)[1]} \\
&+ {}^{1,1[2]}C_{0,1[1]}^{1,2[2]} a_{0,1}^{(1)[1]} a_{1,-2}^{(1)[2]} + {}^{1,1[2]}C_{0,1[2]}^{1,2[1]} a_{0,1}^{(1)[2]} a_{1,-2}^{(1)[1]} - {}^{1,1[2]}C_{1,-2[2]}^{0,1[2]} a_{0,1}^{(1)[2]} a_{1,-2}^{(1)[2]} \\
&- {}^{1,1[2]}C_{1,0[1]}^{0,1[1]} a_{1,0}^{(1)[1]} a_{0,1}^{(1)[1]*} - {}^{1,1[2]}C_{1,0[1]}^{0,1[2]} a_{1,0}^{(1)[1]} a_{0,1}^{(1)[2]*} \\
&+ {}^{1,1[2]}C_{1,-1[1]}^{0,2[1]} a_{1,1}^{(1)[1]} a_{0,2}^{(1)[1]*} + {}^{1,1[2]}C_{1,-1[1]}^{0,2[2]} a_{1,1}^{(1)[1]} a_{0,2}^{(1)[2]*} \\
&+ {}^{1,1[2]}C_{1,-1[2]}^{0,2[1]} a_{1,1}^{(1)[2]} a_{0,2}^{(1)[1]*} \\
&+ {}^{1,1[2]}C_{1,-1[2]}^{0,2[2]} a_{1,1}^{(1)[2]} a_{0,2}^{(1)[2]*} - {}^{1,1[2]}C_{1,-2[1]}^{0,3[1]} a_{1,2}^{(1)[1]} a_{0,3}^{(1)[1]*} \\
&+ {}^{1,1[2]}C_{1,-2[1]}^{0,3[2]} a_{1,2}^{(1)[1]} a_{0,3}^{(1)[2]*} - {}^{1,1[2]}C_{1,-2[2]}^{0,3[1]} a_{1,2}^{(1)[2]} a_{0,3}^{(1)[1]*} \\
&- {}^{1,1[2]}C_{1,-2[2]}^{0,3[2]} a_{1,2}^{(1)[2]} a_{0,3}^{(1)[2]*}
\end{aligned} \tag{5.10}
$$

$$
\begin{aligned}
e_{03}^{[1]}\ \dot{a}_{0,3}^{(1)[1]} &= A_{03}^{'} a_{0,3}^{(1)[1]}/Re + A_{03}^{''} a_{0,3}^{(1)[2]} + B_{03} a_{0,0}^{(1)[1]} a_{0,3}^{(1)[2]} + {}^{0,1[1]}C_{0,2[2]}^{0,3[1]} a_{0,1}^{(1)[1]} a_{0,2}^{(1)[2]} \\
&+ {}^{0,2[1]}C_{0,1[2]}^{0,3[1]} a_{0,1}^{(1)[2]} a_{0,2}^{(1)[1]} + {}^{0,3[1]}C_{1,-2[1]}^{1,1[1]} (a_{1,1}^{(1)[1]} a_{1,-2}^{(1)[1]*} - a_{1,2}^{(1)[1]} a_{1,-1}^{(1)[1]*}) \\
&- {}^{0,3[1]}C_{1,-2[2]}^{1,1[1]} (a_{1,1}^{(1)[1]} a_{1,-2}^{(1)[2]*} - a_{1,2}^{(1)[2]} a_{1,-1}^{(1)[1]*}) \\
&- {}^{0,3[1]}C_{1,-2[1]}^{1,1[2]} (a_{1,1}^{(1)[2]} a_{1,-2}^{(1)[1]*} - a_{1,2}^{(1)[1]} a_{1,1}^{(1)[2]*}) \\
&- {}^{0,3[1]}C_{1,-2[2]}^{1,1[2]} (a_{1,1}^{(1)[2]} a_{1,-2}^{(1)[2]*} - a_{1,2}^{(1)[2]} a_{1,-1}^{(1)[2]*})
\end{aligned} \tag{5.11}
$$

$$
\begin{aligned}
e_{03}^{[2]}\ \dot{a}_{0,3}^{(1)[2]} &= A_{03}^{'''} a_{0,3}^{(1)[2]}/Re + {}^{0,3[2]}C_{0,2[2]}^{0,1[2]} a_{0,1}^{(1)[2]} a_{0,2}^{(1)[2]} + {}^{0,3[2]}C_{1,-2[1]}^{1,1[1]} a_{1,1}^{(1)[1]} a_{1,-2}^{(1)[1]*} \\
&- {}^{0,3[2]}C_{1,-2[2]}^{1,1[1]} (a_{1,1}^{(1)[1]} a_{1,-2}^{(1)[2]*} - a_{1,2}^{(1)[2]} a_{1,-1}^{(1)[1]*}) - {}^{0,3[2]}C_{1,-1[1]}^{1,2[1]} a_{1,2}^{(1)[1]} a_{1,-1}^{(1)[1]*} \\
&+ {}^{0,3[2]}C_{1,-2[1]}^{1,1[2]} (a_{1,1}^{(1)[2]} a_{1,-2}^{(1)[1]*} - a_{1,2}^{(1)[1]} a_{1,-1}^{(1)[2]*}) \\
&- {}^{0,3[2]}C_{1,-2[2]}^{1,1[2]} (a_{1,1}^{(1)[2]} a_{1,-2}^{(1)[2]*} - a_{1,2}^{(1)[2]} a_{1,-1}^{(1)[2]*})
\end{aligned} \tag{5.12}
$$

$$
\begin{aligned}
e_{12}^{[1]}\ \dot{a}_{1,2}^{(1)[1]} &= A_{12}^{'} a_{1,2}^{(1)[1]}/Re + A_{12}^{''} a_{1,2}^{(1)[2]} - B_{12}^{[1]} a_{0,0}^{(1)[1]} a_{1,2}^{(1)[2]} + {}^{1,2[1]}C_{1,1[1]}^{0,1[1]} a_{0,1}^{(1)[1]} a_{1,1}^{(1)[1]} \\
&- {}^{1,2[1]}C_{1,1[2]}^{0,1[1]} a_{0,1}^{(1)[1]} a_{1,1}^{(1)[2]} + {}^{1,2[1]}C_{1,1[1]}^{0,1[2]} a_{0,1}^{(1)[2]} a_{1,1}^{(1)[1]} + {}^{1,2[1]}C_{1,1[2]}^{0,1[2]} a_{0,1}^{(1)[2]} a_{1,1}^{(1)[2]} \\
&+ {}^{1,2[1]}C_{1,0[1]}^{0,2[1]} a_{0,2}^{(1)[1]} a_{1,0}^{(1)[1]} + {}^{1,2[1]}C_{1,0[1]}^{0,2[2]} a_{0,2}^{(1)[2]} a_{1,0}^{(1)[1]} + {}^{1,2[1]}C_{0,3[1]}^{1,-1[1]} a_{1,-1}^{(1)[1]} a_{0,3}^{(1)[1]} \\
&- {}^{1,2[1]}C_{0,3[2]}^{1,-1[1]} a_{1,-1}^{(1)[1]} a_{0,3}^{(1)[2]} - {}^{1,2[1]}C_{0,3[1]}^{1,-1[2]} a_{1,-1}^{(1)[2]} a_{0,3}^{(1)[1]} \\
&- {}^{1,2[1]}C_{0,3[2]}^{1,-1[2]} a_{1,-1}^{(1)[2]} a_{0,3}^{(1)[2]}
\end{aligned} \tag{5.13}
$$

$$
\begin{aligned}
e_{12}^{[2]}\ \dot{a}_{1,2}^{(1)[2]} &= A_{12}^{'''} a_{1,2}^{(1)[2]}/Re + A_{12}^{''''} a_{1,2}^{(1)[2]} - 0.5 B_{12}^{[2]} a_{0,0}^{(1)[1]} a_{1,2}^{(1)[2]} + {}^{1,2[2]}C_{1,1[1]}^{0,1[1]} a_{0,1}^{(1)[1]} a_{1,1}^{(1)[1]} \\
&+ {}^{1,2[2]}C_{1,1[2]}^{0,1[1]} a_{0,1}^{(1)[1]} a_{1,1}^{(1)[2]} - {}^{1,2[2]}C_{1,1[1]}^{0,1[2]} a_{0,1}^{(1)[2]} a_{1,1}^{(1)[1]} - {}^{1,2[2]}C_{1,1[2]}^{0,1[2]} a_{0,1}^{(1)[2]} a_{1,1}^{(1)[2]} \\
&+ {}^{1,2[2]}C_{1,0[1]}^{0,2[1]} a_{0,2}^{(1)[1]} a_{1,0}^{(1)[1]} - {}^{1,2[2]}C_{1,0[1]}^{0,2[2]} a_{0,2}^{(1)[2]} a_{1,0}^{(1)[1]} - {}^{1,2[2]}C_{0,3[1]}^{1,-1[1]} a_{1,-1}^{(1)[1]} a_{0,3}^{(1)[1]} \\
&- {}^{1,2[2]}C_{0,3[2]}^{1,-1[1]} a_{1,-1}^{(1)[1]} a_{0,3}^{(1)[2]} + {}^{1,2[2]}C_{0,3[1]}^{1,-1[2]} a_{1,-1}^{(1)[2]} a_{0,3}^{(1)[1]} \\
&+ {}^{1,2[2]}C_{0,3[2]}^{1,-1[2]} a_{1,-1}^{(1)[2]} a_{0,3}^{(1)[2]}
\end{aligned} \tag{5.14}
$$

$$
\begin{aligned}
e_{12}^{[1]}\ \dot{a}_{1,-2}^{(1)[1]} = {} & A_{12}^{'} a_{1,-2}^{(1)[1]}/Re + A_{12}^{''} a_{1,-2}^{(1)[2]} - B_{12}^{[1]} a_{0,0}^{(1)[1]} a_{1,-2}^{(1)[2]} + {}^{1,2[1]}C_{1,0[1]}^{0,2[1]} a_{1,0}^{(1)[1]} a_{0,2}^{(1)[1]*} \\
& + {}^{1,2[1]}C_{1,0[1]}^{0,2[2]} a_{1,0}^{(1)[1]} a_{0,2}^{(1)[2]*} - {}^{1,2[1]}C_{0,3[1]}^{1,-1[1]} a_{1,1}^{(1)[1]} a_{0,3}^{(1)[1]*} \\
& + {}^{1,2[1]}C_{0,3[2]}^{1,-1[1]} a_{1,1}^{(1)[1]} a_{0,3}^{(1)[2]*} + {}^{1,2[1]}C_{0,3[1]}^{1,-1[2]} a_{1,1}^{(1)[2]} a_{0,3}^{(1)[1]*} \\
& + {}^{1,2[1]}C_{0,3[2]}^{1,-1[2]} a_{1,1}^{(1)[2]} a_{0,3}^{(1)[2]*} - {}^{1,2[1]}C_{1,1[1]}^{0,1[1]} a_{1,-1}^{(1)[1]} a_{0,1}^{(1)[1]*} \\
& - {}^{1,2[1]}C_{1,1[1]}^{0,1[2]} a_{1,-1}^{(1)[1]} a_{0,1}^{(1)[2]*} + {}^{1,2[1]}C_{1,1[2]}^{0,1[1]} a_{1,-1}^{(1)[2]} a_{0,1}^{(1)[1]*} \\
& - {}^{1,2[1]}C_{1,1[2]}^{0,1[2]} a_{1,-1}^{(1)[2]} a_{0,1}^{(1)[2]*}
\end{aligned} \tag{5.15}
$$

$$
\begin{aligned}
e_{12}^{[2]}\ \dot{a}_{1,-2}^{(1)[2]} = {} & A_{12}^{'''} a_{1,-2}^{(1)[2]}/Re + A_{12}^{''''} a_{1,-2}^{(1)[2]} - 0.5 B_{12}^{[2]} a_{0,0}^{(1)[1]} a_{1,-2}^{(1)[2]} \\
& + {}^{1,2[2]}C_{1,0[1]}^{0,2[1]} a_{1,0}^{(1)[1]} a_{0,2}^{(1)[1]*} - {}^{1,2[2]}C_{1,0[1]}^{0,2[2]} a_{1,0}^{(1)[1]} a_{0,2}^{(1)[2]*} \\
& + {}^{1,2[2]}C_{0,3[1]}^{1,-1[1]} a_{1,1}^{(1)[1]} a_{0,3}^{(1)[1]*} + {}^{1,2[2]}C_{0,3[2]}^{1,-1[1]} a_{1,1}^{(1)[1]} a_{0,3}^{(1)[2]*} \\
& - {}^{1,2[2]}C_{0,3[1]}^{1,-1[2]} a_{1,1}^{(1)[2]} a_{0,3}^{(1)[1]*} - {}^{1,2[2]}C_{0,3[2]}^{1,-1[2]} a_{1,1}^{(1)[2]} a_{0,3}^{(1)[2]*} \\
& - {}^{1,2[2]}C_{1,1[1]}^{0,1[1]} a_{1,-1}^{(1)[1]} a_{0,1}^{(1)[1]*} + {}^{1,2[2]}C_{1,1[1]}^{0,1[2]} a_{1,-1}^{(1)[1]} a_{0,1}^{(1)[2]*} \\
& - {}^{1,2[2]}C_{1,1[2]}^{0,1[1]} a_{1,-1}^{(1)[2]} a_{0,1}^{(1)[1]*} + {}^{1,2[2]}C_{1,1[2]}^{0,1[2]} a_{1,-1}^{(1)[2]} a_{0,1}^{(1)[2]*}
\end{aligned} \tag{5.16}
$$

$$e_{01}^{[1]} = 0.9425, \quad e_{01}^{[2]} = 0.0575, \quad e_{02}^{[1]} = 0.9943, \quad e_{02}^{[2]} = 0.0057, \quad e_{03}^{[1]} = 0.9963$$

$$e_{03}^{[2]} = 0.0037, \quad e_{11}^{[1]} = 0.8744, \quad e_{11}^{[2]} = 0.1256, \quad e_{12}^{[1]} = 0.8977, \quad e_{12}^{[2]} = 0.1023$$

$$A_{00} = -10.760, \quad A_{01}^{'} = -9.269, \quad A_{01}^{''} = 0.1281, \quad A_{01}^{'''} = -0.5567$$

$$A_{02}^{'} = -21.6678, \quad A_{02}^{''} = -0.0503, \quad A_{02}^{'''} = -0.2163, \quad A_{10} = 9.9411$$

$$A_{11}^{'} = -8.3273, \quad A_{11}^{''} = 0.0267, \quad A_{11}^{'''} = -6.7573, \quad A_{11}^{''''} = -0.0126$$

$$A_{03}^{'} = -27.8530, \quad A_{03}^{''} = -0.0563, \quad A_{03}^{'''} = -0.1143$$

$$A_{12}^{'} = -16.2213, \quad A_{12}^{''} = 0.2393, \quad A_{12}^{'''} = -2.1435, \quad A_{12}^{''''} = 0.0037$$

$$B_{01} = 0.0386, \quad B_{02} = 0.0074, \quad B_{03} = 0.0226,$$

$$B_{11}^{[1]} = 0.0009, \quad B_{11}^{[2]} = 0.0004, \quad B_{12}^{[1]} = 0.0856, \quad B_{12}^{[2]} = 0.0040$$

$${}^{0,1[1]}C_{0,1[2]}^{0,2[1]} = 0.0642, \quad {}^{0,1[1]}C_{1,-1[1]}^{1,0[1]} = 0.1782, \quad {}^{0,1[1]}C_{1,-1[2]}^{1,0[1]} = 0.0145,$$

$${}^{0,1[1]}C_{1,-2[1]}^{1,-1[1]} = 0.1626, \quad {}^{0,1[1]}C_{1,-2[2]}^{1,-1[1]} = 0.0001, \quad {}^{0,1[1]}C_{1,-2[1]}^{1,-1[2]} = 0.0073,$$

$${}^{0,1[1]}C_{1,-2[2]}^{1,-1[2]} = 0.0058, \quad {}^{0,1[1]}C_{0,2[2]}^{0,3[1]} = 0.0008, \quad {}^{0,1[1]}C_{0,2[1]}^{0,3[2]} = 0.0001,$$

$${}^{0,1[2]}C_{0,1[2]}^{0,2[2]} = 0.0005, \quad {}^{0,1[2]}C_{1,-1[1]}^{1,0[1]} = 0.0078, \quad {}^{0,1[2]}C_{1,-1[2]}^{1,0[1]} = 0.0136,$$

$${}^{0,1[2]}C_{1,-2[1]}^{1,-1[1]} = 0.0050, \quad {}^{0,1[2]}C_{1,-2[2]}^{1,-1[1]} = 0.0023, \quad {}^{0,1[2]}C_{1,-2[1]}^{1,-1[2]} = 0.0031,$$

$${}^{1,1[1]}C_{0,1[1]}^{1,2[2]} = 0.0044, \quad {}^{0,1[2]}C_{0,2[2]}^{0,3[2]} = 0.0002, \quad {}^{0,2[1]}C_{1,-2[1]}^{1,0[1]} = 0.2250,$$

$${}^{0,2[1]}C_{1,-2[2]}^{1,0[1]} = 0.0125, \quad {}^{0,2[1]}C_{1,-1[2]}^{1,1[1]} = 0.0526, \quad {}^{0,2[1]}C_{1,-1[2]}^{1,1[2]} = 0.0069,$$

$${}^{0,2[1]}C_{0,1[2]}^{0,3[1]} = 0.1511, \quad {}^{0,2[2]}C_{1,-2[1]}^{1,0[1]} = 0.0095, \quad {}^{0,2[2]}C_{1,-2[2]}^{1,0[1]} = 0.0021,$$

$$
\begin{aligned}
&{}^{0,2[2]}C^{1,1[1]}_{1,-1[1]} = 0.0065, \quad {}^{0,2[2]}C^{1,1[1]}_{1,-1[2]} = 0.0056, \quad {}^{0,2[2]}C^{1,1[2]}_{1,-1[2]} = 0.0023,\\
&{}^{0,2[2]}C^{0,3[2]}_{0,1[2]} = 0.0005, \quad {}^{1,0[1]}C^{0,1[2]}_{1,-1[1]} = 0.0170, \quad {}^{1,0[1]}C^{0,1[1]}_{1,-1[1]} = 0.0833,\\
&{}^{1,0[1]}C^{0,1[2]}_{1,-1[2]} = 0.0150, \quad {}^{1,0[1]}C^{0,2[1]}_{1,-2[1]} = 0.0263, \quad {}^{1,0[1]}C^{0,2[2]}_{1,-2[1]} = 0.0005,\\
&{}^{1,0[1]}C^{0,2[2]}_{1,-2[2]} = 0.0024, \quad {}^{1,1[1]}C^{0,1[1]}_{1,0[1]} = 0.0949, \quad {}^{1,1[1]}C^{0,1[2]}_{1,0[1]} = 0.0248,\\
&{}^{1,1[1]}C^{0,2[1]}_{1,-1[2]} = 0.0165, \quad {}^{1,1[1]}C^{0,2[2]}_{1,-1[1]} = 0.0033, \quad {}^{1,1[1]}C^{0,2[2]}_{1,-1[2]} = 0.0047,\\
&{}^{1,1[1]}C^{0,3[1]}_{1,-2[1]} = 0.2969, \quad {}^{1,1[1]}C^{0,3[1]}_{1,-2[2]} = 0.0259, \quad {}^{1,1[1]}C^{0,3[2]}_{1,-2[1]} = 0.0040,\\
&{}^{1,1[1]}C^{0,3[2]}_{1,-2[2]} = 0.0009, \quad {}^{1,1[1]}C^{1,2[1]}_{0,1[1]} = 0.1880, \quad {}^{1,1[1]}C^{1,2[1]}_{0,1[2]} = 0.0302,\\
&{}^{1,1[1]}C^{1,2[2]}_{0,1[2]} = 0.0070, \quad {}^{1,2[2]}C^{1,-1[2]}_{0,3[1]} = 0.0033, \quad {}^{1,2[2]}C^{1,-1[2]}_{0,3[2]} = 0.0016\\
&{}^{1,1[2]}C^{0,1[1]}_{1,0[1]} = 0.0289, \quad {}^{1,1[2]}C^{0,1[2]}_{1,0[1]} = 0.0045, \quad {}^{1,1[2]}C^{0,2[1]}_{1,-1[1]} = 0.0361,\\
&{}^{1,1[2]}C^{0,2[1]}_{1,-1[2]} = 0.0035, \quad {}^{1,1[2]}C^{0,2[2]}_{1,-1[1]} = 0.0009, \quad {}^{1,1[2]}C^{0,2[2]}_{1,-1[2]} = 0.0011,\\
&{}^{1,1[2]}C^{0,3[1]}_{1,-2[1]} = 0.0307, \quad {}^{1,1[2]}C^{0,3[1]}_{1,-2[2]} = 0.0076, \quad {}^{1,1[2]}C^{0,3[2]}_{1,-2[1]} = 0.0012,\\
&{}^{1,1[2]}C^{0,3[2]}_{1,-2[2]} = 0.0017, \quad {}^{1,1[2]}C^{1,2[1]}_{0,1[1]} = 0.0015, \quad {}^{1,1[2]}C^{1,2[1]}_{0,1[2]} = 0.00432\\
&{}^{1,1[2]}C^{1,2[2]}_{0,1[1]} = 0.00136, \quad {}^{1,1[2]}C^{0,1[2]}_{1,-2[2]} = 0.0029, \quad {}^{0,3[1]}C^{1,1[1]}_{1,-2[1]} = 0.1965,\\
&{}^{0,3[1]}C^{1,1[1]}_{1,-2[2]} = 0.0279, \quad {}^{0,3[1]}C^{1,1[2]}_{1,-2[1]} = 0.0532, \quad {}^{0,3[1]}C^{1,1[2]}_{1,-2[2]} = 0.00434,\\
&{}^{0,3[2]}C^{0,1[2]}_{0,2[2]} = 0.0003, \quad {}^{0,3[2]}C^{1,1[1]}_{1,-2[1]} = 0.0018, \quad {}^{0,3[2]}C^{1,1[1]}_{1,-2[2]} = 0.0074,\\
&{}^{0,3[2]}C^{1,1[2]}_{1,-2[1]} = 0.0001, \quad {}^{0,3[2]}C^{1,1[2]}_{1,-2[2]} = 0.000026, \quad {}^{0,3[2]}C^{1,2[1]}_{1,-1[1]} = 0.0018,\\
&{}^{1,2[1]}C^{0,1[1]}_{1,1[1]} = 0.0254, \quad {}^{1,2[1]}C^{0,1[1]}_{1,1[2]} = 0.0088, \quad {}^{1,2[1]}C^{0,1[2]}_{1,1[1]} = 0.0352,\\
&{}^{1,2[1]}C^{0,1[2]}_{1,1[2]} = 0.0012, \quad {}^{1,2[1]}C^{0,2[1]}_{1,0[1]} = 0.1987, \quad {}^{1,2[1]}C^{0,2[2]}_{1,0[1]} = 0.0099,\\
&{}^{1,2[1]}C^{1,-1[2]}_{0,3[1]} = 0.4934, \quad {}^{1,2[1]}C^{1,-1[1]}_{0,3[2]} = 0.0022, \quad {}^{1,2[1]}C^{1,-1[2]}_{0,3[1]} = 0.0225,\\
&{}^{1,2[1]}C^{1,-1[2]}_{0,3[2]} = 0.0012, \quad {}^{1,2[2]}C^{0,1[1]}_{1,1[1]} = 0.0044, \quad {}^{1,2[2]}C^{0,1[1]}_{1,1[2]} = 0.0072,\\
&{}^{1,2[2]}C^{0,1[2]}_{1,1[1]} = 0.0093, \quad {}^{1,2[2]}C^{0,1[2]}_{1,1[2]} = 0.0029, \quad {}^{1,2[2]}C^{0,2[1]}_{1,0[1]} = 0.0250,\\
&{}^{1,2[2]}C^{0,2[2]}_{1,0[1]} = 0.0045, \quad {}^{1,2[2]}C^{1,-1[1]}_{0,3[1]} = 0.0020, \quad {}^{1,2[2]}C^{1,-1[1]}_{0,3[2]} = 0.0066,
\end{aligned}
$$

The $e^{[m]}_{n_x,n_z}$ coefficients on the left hand side of the above ODEs result from the fact that the uncoupled modes are no longer orthonormal, but are merely orthogonal.

REFERENCES

Aubry, N., Holmes, P., Lumley, J. L. & Stone, E. 1988 The dynamics of coherent structures in the wall region of the turbulent boundary layer. *J. Fluid Mech.* **192**, 115–73.

Aubry, N., Lian, W.-Y. & Titi, E. S. 1993 Preserving symmetries in the proper orthogonal decomposition. *SIAM J. on Sci. Comput.* **14**, 483–505.

Baggett, J. S. & Trefethen, L. N. 1997 Low-dimensional models of subcritical transition to turbulence. *Phys. Fluids* **9**, 1043–53.

Bech, K. H., Tillmark, N., Alfredsson, P. H. & Andersson, H. I. 1995 An investigation of turbulent plane Couette flow at low Reynolds numbers. *J. Fluid Mech.* **286**, 291–325.

Berkooz, G., Holmes, P. & Lumley, J. L. 1991 Intermittent dynamics in simple models of the wall layer. *J. Fluid Mech.* **230**, 75–95.

Berkooz, G., Holmes, P. & Lumley, J. L. 1993 The proper orthogonal decomposition in the analysis of turbulent flows. *Ann. Rev. Fluid Mech.* **25**, 539–75.

Berkooz, G. & Titi, E. S. 1993 Galerkin projections and the proper orthogonal decomposition for equivariant equations. *Phys. Lett. A* **174**, 94–102.

Clever, R. M. & Busse, F. H. 1992 Three-dimensional convection in a horizontal fluid layer subjected to a constant shear. *J. Fluid Mech* **234**, 511–27.

Dauchot, O. & Daviaud, F. 1995*a* Finite amplitude perturbation and spots growth mechanism in plane Couette flow. *Phys. Fluids* **7** (2), 335–43.

Dauchot, O. & Daviaud, F. 1995*b* Streamwise vortices in plane Couette flow. *Phys. Fluids* **7**, 901–3.

Dauchot, O. & Vioujard, N. 2000 Phase space analysis of a dynamical model for the subcritical transition to turbulence in plane Couette flow. *Eur. Phys. J. B* **14**, 377–81.

Doedel, E., Champneys, A., Fairgrieve, T., Kuznetsov, Y., Sandstede, B. & Wang, X. 1997 *AUTO 97: Continuation and bifurcation software for ordinary differential equations.* Available via FTP from directory /pub/doedel/auto at ftp.cs.concordia.ca.

Drazin, P. G. & Reid, W. H. 1981 *Hydrodynamic Stability.* Cambridge, UK: Cambridge University Press.

Eckhardt, B., Faisst, H. & Moehlis, J. 2004 A low dimensional model for shear flows. In preparation.

Eckhardt, B. & Mersmann, A. 1999 Transition to turbulence in a shear flow. *Phys. Rev. E* **60**, 509–17.

Gibson, J. 2002 Dynamical systems models of wall-bounded, shear-flow turbulence. PhD thesis, Cornell University.

Hamilton, J., Kim, J. & Waleffe, F. 1995 Regeneration mechanisms of near-wall turbulence structures. *J. Fluid Mech.* **287**, 317–48.

Holmes, P. 1990 Can dynamical systems approach turbulence? In *Whither Turbulence? Turbulence at the Crossroads* (ed. J. L. Lumley), pp. 195–249. New York: Springer-Verlag.

Holmes, P., Lumley, J. L. & Berkooz, G. 1996 *Turbulence, Coherent Structures, Dynamical Systems and Symmetry.* Cambridge, UK: Cambridge University Press.

Jiminez, J. & Moin, P. 1991 The minimal flow unit in near-wall turbulence. *J. Fluid Mech.* **225**, 213–40.

Kawahara, G. & Kida, S. 2001 Periodic motion embedded in plane Couette turbulence: regeneration cycle and burst. *J. Fluid Mech.* **449**, 291–300.

Kim, J., Moin, P. & Moser, R. 1987 Turbulent statistics in fully developed channel flow at low Reynolds number. *J. Fluid Mech.* **177**, 133–66.

Kline, S. J. 1967 The structure of turbulent boundary layers. *J. Fluid Mech.* **30**, 741–73.

Komminaho, J., Lundbladh, A. & Johansson, A. V. 1996 Very large structures in plane turbulent Couette flow. *J. Fluid Mech.* **320**, 259–85.

Lomont, J. S. 1993 *Applications of Finite Groups.* New York, NY: Dover.

Lumley, J. L. 1971 *Stochastic Tools in Turbulence.* New York, NY: Academic Press.

Moehlis, J., Smith, T. R., Holmes, P. & Faisst, H. 2002 Models for turbulent plane Couette flow using the proper orthogonal decomposition. *Phys. Fluids* **14(7)**, 2493–507.

Moffatt, H. K. 1990 Fixed points of turbulent dynamical systems and suppression of nonlinearity. In *Whither Turbulence? Turbulence at the Crossroads* (ed. J. L. Lumley), pp. 250–57. New York: Springer-Verlag.

Nagata, M. 1990 Three-dimensional finite-amplitude solutions in plane Couette flow: bifurcation from infinity. *J. Fluid Mech.* **217**, 519–27.

Peyret, R. 2002 *Spectral Methods for Incompressible Viscous Flow.* New York, NY: Springer-Verlag.

Podvin, B. 2001 On the adequacy of the ten-dimensional model for the wall layer. *Phys. Fluids* **13**, 210–24.

Podvin, B. & Lumley, J. 1998 A low-dimensional approach for the minimal flow unit. *J. Fluid Mech.* **362**, 121–55.

Pope, S. 2000 *Turbulent Flows*. Cambridge, UK: Cambridge University Press.

Sanghi, S. & Aubry, N. 1993 Mode interaction models for near-wall turbulence. *J. Fluid Mech.* **247**, 455–88.

Schmid, P. J. & Henningson, D. S. 2000 *Stability and Transition in Shear Flows*. New York, NY: Springer-Verlag.

Schmiegel, A. 1999 Transition to turbulence in linearly stable shear flows. PhD thesis, Universität Marburg.

Schmiegel, A. & Eckhardt, B. 1997 Fractal stability border in plane Couette flow. *Phys. Rev. Lett.* **79** (26), 5250–3.

Sirovich, L. 1987 Turbulence and the dynamics of coherent structures, parts I-III. *Quart. Appl. Math.* **XLV** (3), 561–82.

Smith, T. R. 2003 Low-dimensional models of plane Couette flow using the proper orthogonal decomposition. PhD thesis, Princeton University.

Smith, T. R., Moehlis, J. & Holmes, P. 2004 Heteroclinic cycles and periodic orbits for the O(2)-equivariant 0:1:2 mode interaction. In preparation.

Trefethen, L. N. 1992 Pseudospectra of matrices. In *Numerical Analysis 1991* (ed. D. F. Griffiths & G. A. Watson), pp. 234–266. Harlow, Essex, UK: Longman Sci. Tech.

Trefethen, L. N., Trefethen, A. E., Reddy, S. & Driscoll, T. 1993 Hydrodynamic stability without eigenvalues. *Science* **261**, 578–84.

Waleffe, F. 1995*a* Hydrodynamic stability and turbulence: beyond transients to a self-sustaining process. *Stud. Appl. Math.* **95**, 319–43.

Waleffe, F. 1995*b* Transition in shear flows. Nonlinear normality versus non-normal linearity. *Phys. Fluids* **7** (12), 3060–6.

Waleffe, F. 1997 On a self-sustaining process in shear flows. *Phys. Fluids* **9**, 883–900.

Zang, T. A. & Hussaini, M. Y. 1985 Numerical experiments on subcritical transition mechanisms. *AIAA paper* **85-0296**, 1–18.